

Chapter 2

Fundamentals of Statics of Masonry Solids and Structures

Abstract Groundings of statics of masonry solids and structures are the subject of the chapter. Masonry behavior is strongly influenced by the dramatically lower strength in tension than in compression. Masonry structures can thus suffer cracks generating displacement fields, called *mechanisms*, which develop without any internal opposition of the material. Collapse can occur without any material failure. The Heyman masonry model, the idealized rigid in compression no tension material, is fruitfully assumed as basis of the approach followed in the chapter. The extension of this model to the masonry continuum is then developed. Strains and detachments occurring in a no tension masonry solid can thus obtain a suitable mathematical definition together with the admissible equilibrium. Both a proper virtual work equation, that considers the boundary of the body including the crack surfaces, as a condition on the loads, necessary and sufficient to the existence of the masonry equilibrium, can be formulated. This last condition governs the collapse strength of masonry structures. The notion of the minimum thrust, from both static and kinematical approaches, is then introduced, widening the field of application of the Limit Analysis also to the study of the actual stress states. A critical analysis of the recent failure of the cathedral of Noto, in Sicily (Italy), useful to a better understanding of the above discussed mechanical concepts, ends the chapter.

2.1 Introduction

Under a given loading path, a masonry structure can reach a collapse condition solely due to loss of equilibrium, that is to say, in the absence of any material failure. Such a condition can therefore arise even in masonry with infinite compression strength. As discussed in the previous chapter, the tensile strength of masonry is, in fact, very low, near zero. Consequently, masonry structures can suffer cracks or detachments that may in turn generate displacement fields, often called *mechanisms*, which develop without any internal opposition from the material.

As soon as the pushing loads begin to exceed the action of the resistant loads along one of these mechanisms, the structure fails. It is thus easy to understand how the presence of negligible tensile strength can disrupt the behavior of structures as compared to the common elastic ones.

Clearly, other failure modes can occur, such as those depending on the compression strength of the material, described in Chap. 1, or those involving the destabilizing effects of axial loads, covered in Chap. 6. However, this first collapse mode affects a wide variety of structures and is, in practice, the most relevant. It stems from the essential aspects of the behavior of masonry structures, aspects which were fully understood by ancient builders, and which have therefore shaped the course of architecture since the origins up to the 19th century.

The aim of this chapter is to analyze these issues involved in such failure mechanisms. The choice of the most convenient model to use for masonry materials will be addressed first. Any model for describing masonry behavior must be as simple as possible, but at the same time be able to represent its most salient aspects. In this regard, the ingenious Heyman model of masonry as a no-tension material that is rigid under compression (1966) is the most satisfactory for our purposes and will be discussed in the following and constantly referred to throughout this book.

2.2 No-Tension Masonry Models

2.2.1 *No-Tension Assumption*

There are sound reasons for adopting the assumption of no tensile strength in masonry. First of all, as evidenced in the previous chapter, most masonry materials exhibit very low tensile strength. This is due, rather than to the mortar's low tensile strength, to the very low adhesion between mortar and bricks, which thus represents the weakest link. Moreover, the mortar in historic constructions may be very poor. Masonry may, in some exceptional cases, exhibit non-negligible tensile strength and its behavior could, at first sight, be modeled as a traditional elastic material. However, random dynamic actions, which can produce cracks in the masonry mass, will eventually cause the material to revert to no-tension behavior.

The effects of subsequent slow penetration of humidity into the cracks can then make things even worse. In such cases, it is possible that a masonry structure which in its pristine state is able to sustain the action of given loads by virtue of its initial non-negligible tensile strength, will not be able to sustain the same loads later, when this strength is fading. In such cases the long-term behavior of masonry can be conservatively assumed to follow the no-tension model. A number of examples, some quite striking, will be discussed in the following.

To sum up then, it is clear that the no-tension assumption is well-grounded. Indeed, it is widely adopted in nearly all the mechanical models proposed for historic masonry structures.

2.2.2 The Problem of Elastic Compressive Strains

In order for any model to adequately describe masonry structures, it must account not only for elastic compressive strains, but for the continuous or discontinuous extensional strains associated with cracking as well.

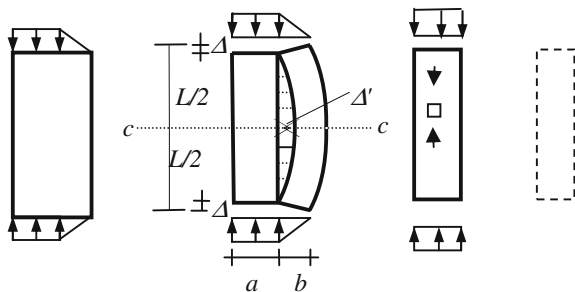
In-depth research studies into the behavior of *elastic no-tension* bodies have been conducted by many authors, among which the works of Di Pasquale (1984), Del Piero (1989), Lucchesi and co-workers (2003), Romano and Romano (1985), Romano and Sacco (1986), Baratta (1982), Angelillo (2010), Trovalusci (1993), Bacigalupo and Gambarotta (2011) etc. All have addressed the general problem of the elastic equilibrium of no-tension bodies and, although numerous, noteworthy stress solutions have been provided (Lucchesi et al. 2008), the much more complex goal of solutions expressed in terms of displacement and strain fields remains incompletely solved to date. The difficulties encountered in this latter research field stem from the fact that the no-tension elastic model cannot easily account for the presence of shear strains. One example in this regard is the masonry panel subjected to bending and axial loads illustrated in Fig. 2.1. The panel, of thickness s , is loaded at its top and base by the pressure p which remains constant along the band a and then varies linearly from p to zero on the remaining band of width b . The borders of the panel are free to deform. The band of width a , under uniform compression p , shortens with respect to the horizontal axis of symmetry, $c-c$. The top sections of the panel band, of width a , move vertically by the amount

$$\Delta = \frac{pasL}{Eas2} = \frac{pL}{E2} \tag{2.1}$$

The side band of width b is axially loaded eccentrically. The left-hand corner of the top section of this band moves vertically and remains in contact with the right-hand corner of the top section of the band of width a . The right-hand band is loaded by the axial load, N , and bending moment, M

$$N = \frac{pbs}{2} \quad M = \frac{pb^2s}{12} \tag{2.2}$$

Fig. 2.1 The behavior of an elastic no-tension panel under variable compressions applied at its *base* and *top* sections



The top section of this band sinks under the action of N and rotates counter clockwise under the bending moment M . The total vertical displacement of left-hand corner of this section is

$$\Delta = \frac{pbs}{2} \frac{L}{2Ebs} + M \frac{12L}{2Esb^3} \frac{b}{2} = \frac{pL}{E4} + \frac{pb^2s}{12} \frac{12L}{2Esb^3} \frac{b}{2} = \frac{pL}{E4} + \frac{pL}{E4} = \frac{pL}{E2} \quad (2.3)$$

which is equal to displacement (2.1). Cracks arise along the vertical line of connection between the two bands. The maximum width Δ' of these discontinuities or detachments is

$$\Delta' = M \frac{12}{2Esb^3} \left(\frac{L}{2}\right)^2 = \frac{pLL}{8Eb} \quad (2.4)$$

Now, as the width b of the band becomes smaller and smaller, at the limit $b \rightarrow 0$, we have

$$\lim_{b \rightarrow 0} \Delta' = \infty \quad (2.5)$$

In particular, if only one band of the panel is uniformly compressed, while the other band is unloaded, the stress state is defined unequivocally. The loaded side is uniformly compressed and the side band remains unloaded. Strains, on the contrary, behave in a singular way. The unloaded side of the panel detaches from the loaded one and tends towards infinity because a no-tension elastic material is unable to accept the presence of shear strains along the contact zone between the loaded and unloaded sides.

None of the linear segments, all contained within the unloaded masonry solid, can in fact be shortened during deformation. This result emphasizes the singular behavior of such panels and raises doubts about the ability of the elastic no-tension model to realistically represent the response of masonry structures partially loaded over their boundaries. By using the rigid in compression no-tension model, which neglects the elastic strains, the solution is more regular. In this case, in place of the diverging solution, the unloaded part of the panel can detach from the loaded part by an arbitrary, but finite quantity (Fig. 2.2).

Neglecting the elastic compression strains has *no influence* on evaluation of the limit loads. Indeed, from the perspective of Limit Analysis, we know that the presence of elastic strains has no effect on the collapse load, except in the event that the changes in geometry become relevant. This question has been thoroughly studied in the general analysis of elastic-plastic bodies. During the onset of the failure mechanism all stresses remain constant and new elastic strains do not develop (Prager 1959). The same occurs for both elastic and rigid no-tension structures, as will be shown in the following (Fig. 2.3).

Currently, only advanced, computationally demanding programs can provide information on the effects of the elastic compressive strains within masonry model of structures by assuming a small finite tensile strength.

Fig. 2.2 The rigid no-tension panel partially compressed at its *base* and *top* sections

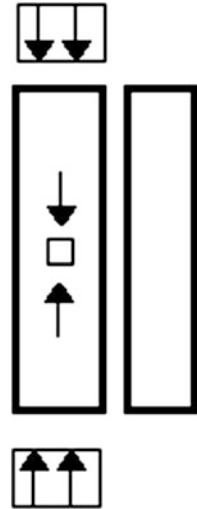
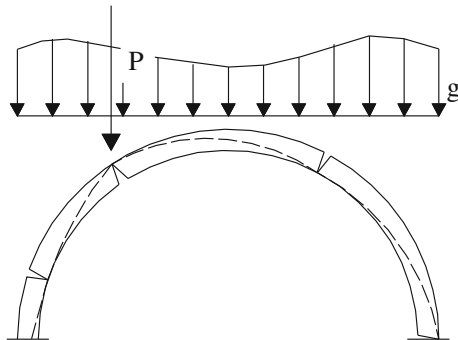


Fig. 2.3 Collapse of the arch



The problem is similar if we want to check the actual equilibrium state. At a first sight the problem can be solved by assuming the *elastic* in compression no tension model that permits to obtain the lacking equations: they express the compatibility of the deformation of the structure with its external environment. On the contrary, the research of equilibrium configuration of the *rigid no tension* masonry structures under a given load distribution becomes *statically undetermined*. The external constraints, representing the structure environment, will suffer a certain amount of deformation, that we will call *settlement*. These deformations can be represented by the settlement of the soil, as in the example of the arch of Fig. 2.4, or by the same deformation of supporting substructures: for instance the deformation of the drum sustaining a dome.

The elastic no tension solution, on the other hand, is dependent on the magnitude of settlement only if this displacement is very small because rapidly it matches the solution corresponding to the rigid no tension model.

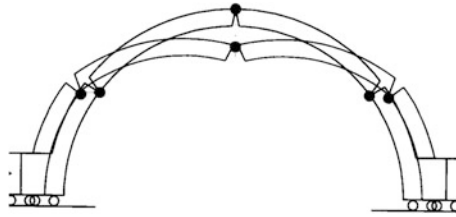


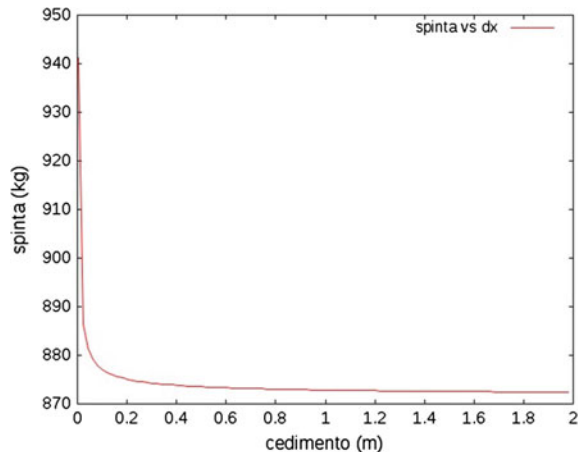
Fig. 2.4 Settlement deformation of the masonry arch

These considerations can be illustrated by the following example regarding the behavior of an arch, studied by assuming the elastic in compression no tension model. The example was studied by N. Zani of the university of Florence. The arch, loaded by its own weight, suffers an horizontal settlement at its springing. It is required to evaluate the variation of the thrust of the arch with the magnitude of the imposed settlement. Figure 2.5 gives the plot of the thrust of the arch versus the magnitude of the imposed settlement.

Starting from the fixed springings condition, the thrust of the arch drops immediately as soon as the settlement occurs and approaches the value of the minimum thrust, about equal to 874 kg, corresponding to the reaching of the mechanism state. Further, Fig. 2.6 shows the pressure lines developing in the arch respectively at the initial state, with fixed springings, and just after the thrust drop.

The assuming the rigid in compression no tension model prevents to describe, during the loading progress, the *gradual* development of cracking in the structure before the reaching the settlement mechanism state. But this phase of working of masonry structures should be *meaningless*, owing to the strong sensitivity of masonry structures to the magnitude of the settlement, as shown by the arch behavior of Fig. 2.5.

Fig. 2.5 Plot of the thrust of the elastic no tension arch versus the horizontal settlement (private communication by N. Zani, Departm. of Constructions, Univ. of Florence, Italy, July 2011)



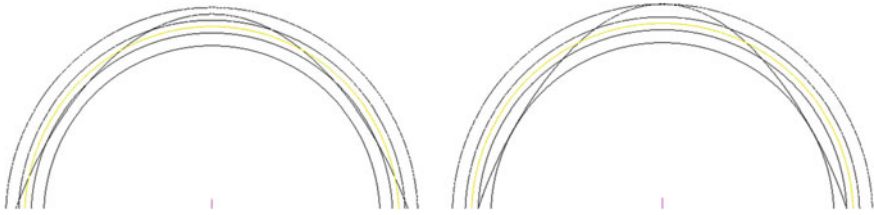


Fig. 2.6 Pressure lines in the elastic no tension arch at its initial state, with fixed springings, and near the mechanism state, just after the thrust drop. (private communication by N. Zani, Departm. of Constructions, Univ. of Florence, Italy, July 2011)

After the settling displacements have reached a certain level, the structure effectively becomes a mechanism and can adjust by maintaining its internal stresses constant. With reference to the example masonry arch in Fig. 2.4, which has undergone a slight increase in span due to settling of its springers, according to Heyman (1995), it can be seen that the arch is able to adapt itself to the settlement by maintaining the stresses constant regardless of the degree of settling.

In studying the real equilibrium states of masonry structures, equivalent results can thus be obtained by applying the rigid no-tension model. As will be shown in the following, the minimum thrust states can provide the additional equations needed to solve the problem. On the wake of this Heyman suggestion, the so called equilibrium approach (Huerta 2001) can permit to tackle with great simplicity the research of the actual set up of masonry structures. In the end, summing up all the previous discussions, we will make reference in our analysis to the rigid no tension Heyman model.

2.3 The Rigid No-Tension Model

2.3.1 *The Heyman's Assumptions*

The constitutive assumptions originally formulated by Heyman (1966) are as follows:

- (i) *masonry is incapable of withstanding tensions;*
- (ii) *masonry has infinite compressive strength;*
- (iii) *elastic strains are negligible;*
- (iv) *slidings cannot occur because masonry has infinite shear strength;*

The corresponding uniaxial stress–strain relation is shown in Fig. 2.7. The first two of Heyman's assumptions above involve stresses; the latter two, strains.

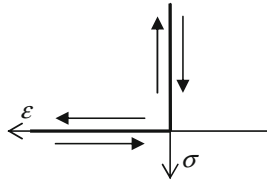


Fig. 2.7 Uniaxial stress–strain relation of rigid no-tension masonry material

2.3.2 The Unit Resistant Masonry Cell

The foregoing assumptions turn out to be very clear if we refer to the elementary resistant cell of the masonry structure, represented by two idealized rigid masonry bricks compressed one against the other by a more or less eccentric axial load and possibly loaded by a shear force (Fig. 2.8).

The two rigid bricks of the unit resistant cell, of height h , cannot deform internally, but they can detach from each other (Fig. 2.9). A crack occurs in the cell.

The overall stress state is determined by an axial force N applied at the section's centre, a moment M and a shear force T . Thus, the stress state acting on the unit cell can be represented by the vector

$$\Sigma = \begin{bmatrix} M \\ N \\ T \end{bmatrix} \tag{2.6}$$

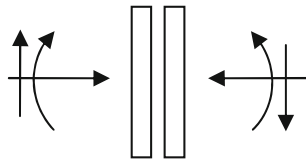


Fig. 2.8 The unit resistant masonry cell

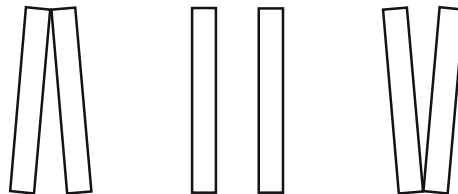


Fig. 2.9 Admissible displacements of the unit cell blocks

According to assumption (i), only compressive stresses are consistent. Thus, the eccentricity of the axial load N

$$e = M/N \tag{2.7}$$

must satisfy the inequalities

$$-h/2 \leq e \leq h/2 \tag{2.8}$$

Assumption (iv) prohibits sliding. Consequently, the shear force T will not be bound by any restrictions. Using the reference system N, M, T , any point in this space thus defines a possible loading condition. Since shear T is uninvolved in defining the limit equilibrium between the two ideal bricks, we can consider the projection Σ' of Σ on the coordinate plane N, M , as shown in Fig. 2.10.

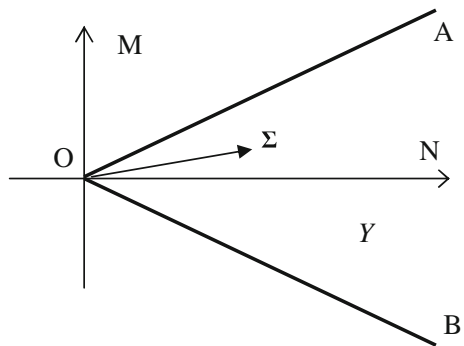
According to (2.8), the eccentric axial loading state, defined by the values of the axial force N and moment M (and which we will continue to indicate as Σ for the sake of simplicity), cannot extend beyond the two limit lines represented in the plane (N, M) by the two straight lines OA and OB in Fig. 2.10.

$$M = N \frac{h}{2} \quad M = -N \frac{h}{2} \tag{2.9}$$

The set of *all consistent stress states* in the space M, N, T is thus the region between the two π planes orthogonal to plane $T = 0$ having intersections with the two limit lines $M = Nh/2$ and $M = -Nh/2$. In particular, region Y of the consistent stress states is the region in plane M, N delimited by angle OAB. Specifically, a vector Σ placed along either line OA or line OB, represents an axial force with eccentricity respectively equal to $h/2$ or $-h/2$, as shown in Fig. 2.11a, b. These peculiar stress states are denoted as Σ_o^+ and Σ_o^- , and are expressed as

$$\Sigma_o^+ = \begin{bmatrix} Nh/2 \\ N \\ T \end{bmatrix} \quad \Sigma_o^- = \begin{bmatrix} -Nh/2 \\ N \\ T \end{bmatrix} \tag{2.10}$$

Fig. 2.10 The region Y of the admissible stresses



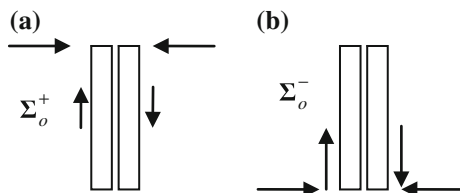


Fig. 2.11 Limit stress states. a, b Limit state

Any deformation of the unit resistant cell will be either zero or a detachment strain and will be represented by the strain vector

$$\mathbf{E} = \begin{bmatrix} \phi \\ \Delta \\ \gamma \end{bmatrix} \tag{2.11}$$

whose components ϕ , Δ and γ are the elementary strains along which the force components M , N and T respectively do work. No strains can occur until the eccentric axial force reaches the upper or the lower edge of the brick cell section (Fig. 2.11a or b).

In the case of Fig. 2.11a, the stress is Σ_o^+ , and the corresponding detachment strain, the vector \mathbf{E}^+ , is produced by the opening of the hinge situated at the upper edge of the section; in the case of Fig. 2.11b, the strain \mathbf{E}^- corresponds to the stress Σ_o^- . These strains are thus defined as

$$\mathbf{E}^+ = \begin{bmatrix} \phi \\ -\phi h/2 \\ 0 \end{bmatrix} \quad \mathbf{E}^- = \begin{bmatrix} -\phi \\ -\phi h/2 \\ 0 \end{bmatrix}. \tag{2.12}$$

Strains (2.12) are kinematically consistent. Stresses at the limit state (+), represented by the vector Σ_o^+ , do not perform work on the corresponding detachment strain \mathbf{E}^+ . Likewise, at the limit state (-), Σ_o^- does no work on the strain \mathbf{E}^- (Fig. 2.12).

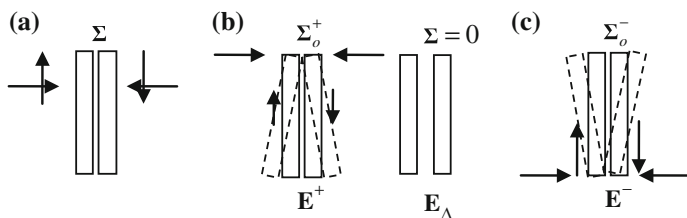


Fig. 2.12 Stress states not producing or producing detachment strains in the cell

In fact

$$\begin{aligned} \Sigma_o^+ \cdot \mathbf{E}^+ &= [Nh/2 \quad N \quad T] \begin{bmatrix} \phi \\ -\phi h/2 \\ 0 \end{bmatrix} = 0 \\ \Sigma_o^- \cdot \mathbf{E}^- &= [-Nh/2 \quad N \quad T] \begin{bmatrix} -\phi \\ -\phi h/2 \\ 0 \end{bmatrix} = 0 \end{aligned} \tag{2.13}$$

The detachment strain \mathbf{E}^+ is thus *orthogonal* to the limit line $M = Nh/2$, while vector \mathbf{E}^- is orthogonal to the other limit line $M = -Nh/2$, as shown in Fig. 2.13. Let us now consider a generic consistent state of stress Σ , that is, within the angular region Y : the resistant cell cannot thus be opened, so the stress Σ cannot do any positive work on any detachment strain \mathbf{E} (Fig. 2.14a). Thus the following inequality holds

$$\Sigma \cdot \mathbf{E} \leq 0, \quad \forall \Sigma \in Y, \tag{2.14}$$

where

$$\Sigma \cdot \mathbf{E} = 0, \tag{2.15}$$

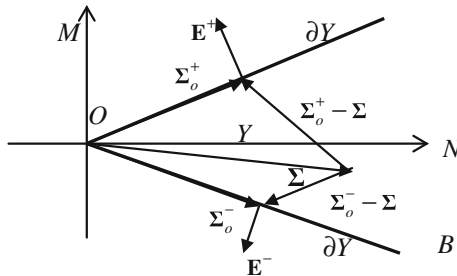


Fig. 2.13 Admissible stress states and detachment strains

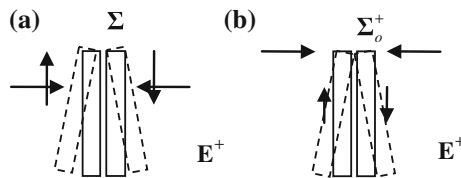


Fig. 2.14 The non-positive work of stresses on the cell strains

iff $\Sigma = \Sigma_o^+$ and $\mathbf{E} = \mathbf{E}^+$, or $\Sigma = \Sigma_o^-$ and $\mathbf{E} = \mathbf{E}^-$, (Fig. 2.14b). In short, we have

$$\Sigma_o^\pm \cdot \mathbf{E}^\pm = 0 \tag{2.16}$$

This last inequality represents the *normality rule* connecting the limit stress with the associated strain vectors. Taking both conditions (2.14) and (2.16) into account, we also have

$$(\Sigma_o^\pm - \Sigma) \cdot \mathbf{E}^\pm \geq 0, \quad \forall \Sigma \in Y \tag{2.17}$$

which shows that the vector

$$(\Sigma_o^\pm - \Sigma)$$

is directed outside region Y , as shown in Fig. 2.13. Inequality (2.17) means that the angle between vectors $(\Sigma_o^\pm - \Sigma)$ and \mathbf{E}^\pm cannot be larger than $\pi/2$.

It is worthwhile examining the case in which all the stresses acting on the cell are equal to zero. In this case, the cell can deform with all its degrees of freedom, as shown in Fig. 2.15. Any consistent deformation of the cell can be expressed by a linear combination of the basic strain components shown in Fig. 2.15: the two strains \mathbf{E}^+ and \mathbf{E}^- and the uniaxial extension \mathbf{E}_Δ . Vector \mathbf{E}^+ , originating at the vertex O of the angular region Y in Fig. 2.11, is orthogonal to the limit line $\Sigma = \Sigma_o^+$; likewise vector \mathbf{E}^- is orthogonal to the limit line $\Sigma = \Sigma_o^-$.

Finally, the uniaxial detachment strain, \mathbf{E}_Δ , is represented by a vector originating at the vertex O and acting along the positive direction of the axis $N(\mathcal{A})$ in Fig. 2.16. The overall strain, obtained by the linear combination of all the three basic vectors \mathbf{E}^+ , \mathbf{E}^- , and \mathbf{E}_Δ , lies within the angular region OAB having its vertex at the origin O and bounded by the lines OA and OB , respectively orthogonal to the limit lines $\Sigma = \Sigma_o^+$ and $\Sigma = \Sigma_o^-$.

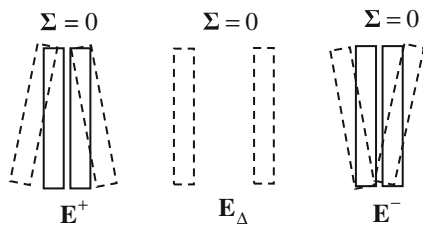
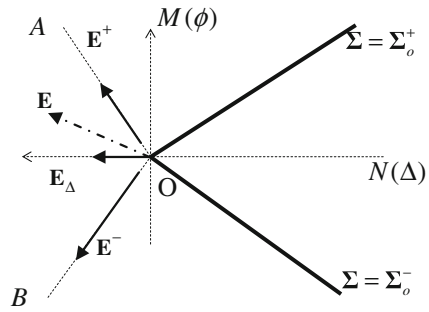


Fig. 2.15 Possible basic strains occurring on the unloaded cell

Fig. 2.16 Overall strain of the unloaded cell as the sum of all the basic strains \mathbf{E}^+ , \mathbf{E}^- and \mathbf{E}_Δ of the cell



2.3.3 Properties of the Rigid No Tension Material

2.3.3.1 Stability

Let us imagine that a consistent stress state Σ_A is applied to the cell by the agent (A) and that another agent, defined as (B), applies additional stresses Σ_B to the cell, so that the overall stress reaches the limit state Σ_o^\pm and the detachment strain ϵ^\pm can occur. The additional stress state Σ_B applied by agent (B) can be expressed as (Fig. 2.17)

$$\Sigma_B = \Sigma_o^\pm - \Sigma_A \tag{2.18}$$

When the \mathbf{E}^\pm occurs, agent (B) does the work $(\Sigma_o^\pm - \Sigma_A) \cdot \mathbf{E}^\pm$ (Fig. 2.17), which according to (2.17) cannot be negative.

The unit masonry cell thus requires that agent (B) expends energy to produce detachment strains. According to Drucker (1959), given the assumed constitutive equation, the masonry material may be defined *stable*. However, the behavior of the material would be quite different if, on the contrary, its constitutive equation were based on friction.

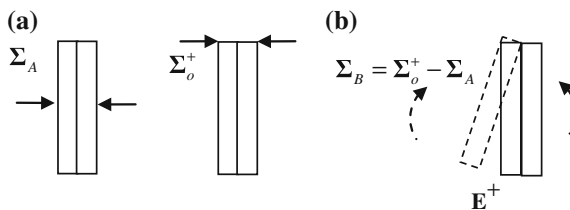
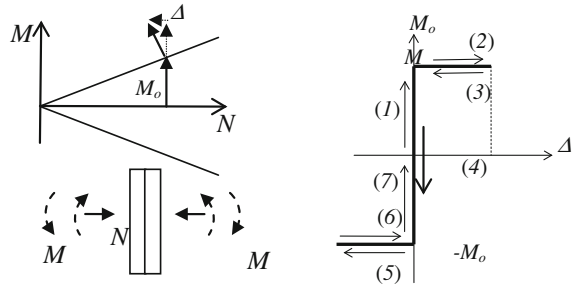


Fig. 2.17 Stresses applied by agent a and subsequent agent b to reach the limit state

Fig. 2.18 Loading and unloading cycles



2.3.3.2 Elasticity

Despite the foregoing results, the difference between masonry behavior and plastic behavior is significant. Even according to the rigid in compression no-tension model, masonry exhibits a behavior that, due to the lack of internal dissipation, can be considered nonlinear elastic. To illustrate, let us examine the unit resistant cell in Fig. 2.18 under a constant axial load N applied by agent (A) and a sequence of loading–unloading cycles of the additional moment M produced by agent (B).

During the first additional loading, due to an increase in moment M , the eccentricity of the axial load N increases gradually and the moment reaches the limit moment M_o , at which point a small detachment strain increment, $\Delta\phi$, ensues. Agent (B) expends energy to produce this strain $\Delta\phi$. Then, in the return cycle, the expended energy is once again *restored* to agent (B) and the diagram of moment M —rotation $\Delta\phi$ takes the form illustrated in Fig. 2.18. Though in many aspects similar to plastic deformations, the occurrence of detachment strains does not involve energy expense. This result highlights a difference between the response of classical elastic-plastic, or rigid-plastic materials, and masonry materials. This question will be taken up again in Chap. 8 by examining some aspects of the dynamic behavior of some elementary masonry structures.

2.3.3.3 The Coulomb Definition of the Masonry Material

The first three previously cited Heyman assumptions, (i), (ii) and (iii), which define the assumed masonry model, can be easily understood as soon as masonry's low tensile strength is taken into account. It is noteworthy, however, that assumption (iv), at first sight very different from the first three, can also be considered as following directly from them (Como and Grimaldi 1985). This can be corroborated in the context of so-called Mohr-Coulomb materials. In fact, with reference to a plane stress state, according to the Coulomb criterion (1773), the shear strength along the plane under the compressive stress σ is (Fig. 2.19)

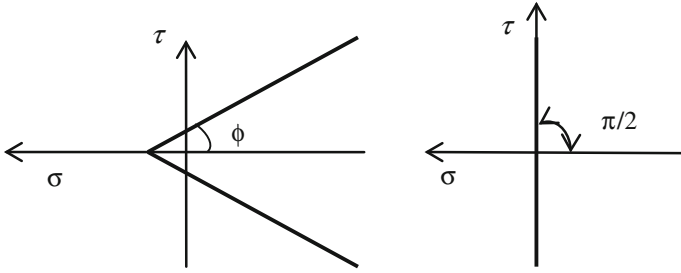


Fig. 2.19 The Coulomb failure criterion, which for $\phi \rightarrow \pi/2$ overlaps the failure criterion of zero maximum tensile stress

$$\tau = c + \sigma \cdot \operatorname{tg} \phi \tag{2.19}$$

where ϕ is the angle of the internal friction. According to the Coulomb criterion, the ratio between uniaxial compressive and tensile stresses takes the form

$$\frac{\sigma_{rc}}{\sigma_{rt}} = \frac{1 + \sin \phi}{1 - \sin \phi} \tag{2.20}$$

By gradually reducing the ratio σ_{rt}/σ_{rc} , at the limit we obtain

$$\frac{\sigma_{rc}}{\sigma_{rt}} \rightarrow \infty \Rightarrow \frac{1 + \sin \phi}{1 - \sin \phi} \rightarrow \infty \Rightarrow \phi \rightarrow \frac{\pi}{2}. \tag{2.21}$$

The two limit lines of the Coulomb criterion, which form angle ϕ with the horizontal axis, become vertical when $\phi \rightarrow \pi/2$ and the Coulomb criterion overlaps the criterion of maximum tensile stress (Fig. 2.19). The internal friction strength becomes unbounded and the condition $\sigma \leq 0$ satisfies assumptions (i) and (ii) above.

2.4 The Masonry Continuum

It can seem strange to use the model of “*continuum*” to describe the mechanical behavior of a material having a discrete structure, composed by bricks or stones and eventually by mortar beds.

This is indeed possible because essentials of the masonry behavior don’t require to specify the internal composition of the material but only its unilateral response, so conditioned by the dramatically lower strength in tension than in compression. This can be made assuming the above discussed basic features of the masonry behavior and the simple model of the material rigid in compression but without tension strength.

According to this no-tension model, a masonry body can be considered an assemblage of rigid particles held together by the compressive stresses produced by loads. The small size of the stones compared to the dimensions of the body enables it to be considered a continuous body instead of a discrete system of many individual particles. When the compression stresses that held stones together cancel out in some regions of the masonry body, it can get deformed. Cracks can thus occur in the masonry mass: they represent discontinuities or detachments of the displacement fields describing the deformation of the body.

The above assumptions of the rigid in compression no-tension model can thus be adopted for the masonry continuum in a more general form by means of suitable conditions that we will go to look for (Como 1992). At the same time, the use of the continuous medium immediately makes the powerful methods of calculus available and able to describe the discontinuous mechanism displacements, due to cracks formation. The study of the failure of masonry bodies due to the cracking development can thus be made in a general form.

In the next sections the compatibility conditions on loads and stresses will be established and then the compatibility conditions for displacements and strain fields.

Various kinds of mechanism displacements can be in fact defined for rigid in compression no tension bodies. Figure 2.20 shows the mechanism displacement due to relative rotations of the three parts in which an arch has been subdivided. In this case no extension strains occur in the arch segments. Figure 2.21 shows the case of the panel that suffers continuous extension strains producing an inner crack.

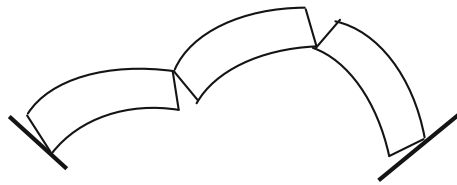


Fig. 2.20 Mechanism induced by rigid rotations of parts of the arch

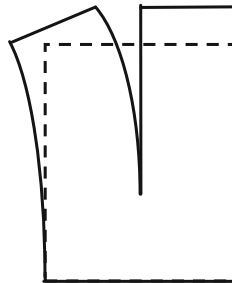


Fig. 2.21 Mechanism induced by extension strains distributed over the upper zone of a panel

2.4.1 Compatibility Conditions on Loads

Let us consider a masonry body occupying the region Ω , whose boundary is denoted as $\partial\Omega$, which we assume to be sufficiently regular (Fig. 2.22). The body is loaded by mass and surface loadings $\rho(\Omega)$ and \mathbf{p} . The loaded part of the body surface $\partial\Omega$ is $\partial\Omega_p$. The surface region $\partial\Omega_r$, is subjected to appropriate boundary conditions. Furthermore, the line f indicates a *crack*. Unlike linear elastic bodies, for masonry structures external loads and internal stresses must necessarily satisfy some compatibility conditions, which are what we are now seeking to define.

For example, tensile forces cannot be applied on the boundary of a no-tension masonry body. Indeed, the surface loads, \mathbf{p} , must be exerted on the surface $\partial\Omega_p$, so that at any point on surface $\partial\Omega_p$ the following condition holds

$$\mathbf{p}(P) \cdot \mathbf{n} \leq 0, \quad \forall P \in \partial\Omega_p \tag{2.22}$$

where \mathbf{n} is the unit vector of the outward normal to $\partial\Omega_p$ at point P .

Likewise, the reactions $\mathbf{r}(P)$ that take place along the boundary $\partial\Omega_r$, will also act on $\partial\Omega_r$, and we thus have

$$\mathbf{r}(P) \cdot \mathbf{n} \leq 0, \quad P \in \partial\Omega_r. \tag{2.23}$$

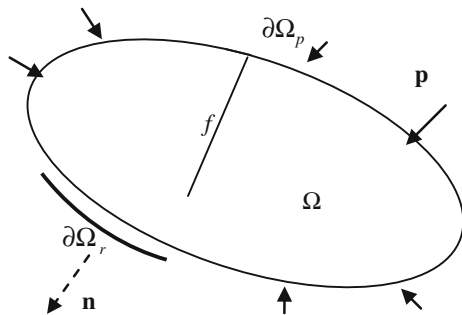
Inequalities (2.22) and (2.23) represent the compatibility conditions on the surface loads \mathbf{p} and reactions \mathbf{r} . As consequence of condition (2.22), *self-equilibrated* load distributions cannot be applied to the masonry body.

2.4.2 Compatibility Conditions on Stresses

Tensile stresses can never develop inside the masonry mass, hence

$$\sigma(P) \leq 0. \tag{2.24}$$

Fig. 2.22 The masonry body occupying the region Ω with boundary $\partial\Omega$



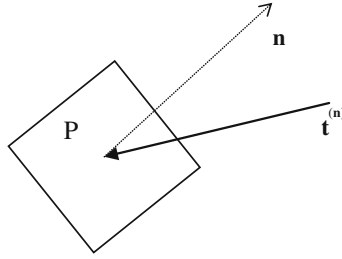


Fig. 2.23 Vector stress on a generic plane without tensile components

Condition (2.24) establishes that at each point P of the body the largest of the principal stresses must be either a compression or equal to zero. Condition (2.24), which was originally formulated by Di Pasquale (1984), defines the domain Y of the statically admissible stress tensors σ .

Let P be an arbitrary point inside the region Ω of the body, dS an oriented surface element passing through P and having the unit vector $\hat{\mathbf{n}}(P)$ on the outward normal originating at P , and $\mathbf{t}^{(n)}(P)$ the associated tension vector representing the force transmitted across the oriented surface element dS . Tensile interactions are not admissible: for any normal $\hat{\mathbf{n}}$ of surface element dS (Fig. 2.23), the following inequality thus holds

$$\mathbf{t}^{(n)}(P) \cdot \hat{\mathbf{n}}(P) \leq 0 \quad (2.25)$$

Apart from restating the material's incapacity to sustain tensile stresses, condition (2.25) also determines several important properties of the stress, which is the topic of the next section.

2.4.3 First Consequence of the No-Tension Assumption

The main consequences of the assumption that masonry materials cannot withstand any tension at all are:

- (1) *Masonry is incompatible with load scattering*
- (2) *The internal resistant structures arising in the body depend on the geometry of the applied loads*

Let us consider a masonry wall loaded only on its inner band, as illustrated in Fig. 2.24. It is immediately evident that *no load scattering*, or dispersion, occurs inside the wall (Di Pasquale 1984). Let us section the wall along the line $a-a$ and consider the equilibrium of the corresponding side band of the wall bounded by the line $a-a$ and the corresponding external edge. By considering the vector stress

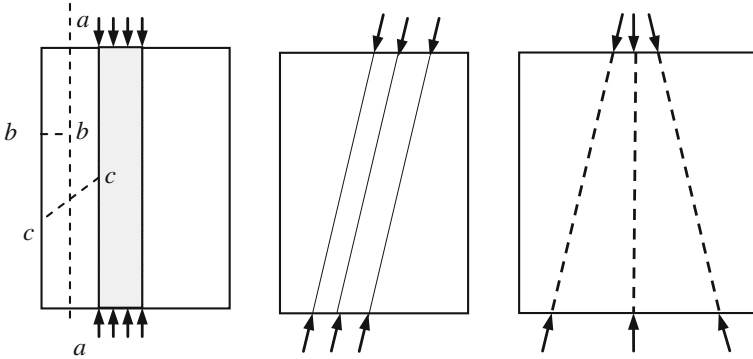


Fig. 2.24 Resistant masonry band without load scattering

$\mathbf{t}^{a-a}(P)$ and its component along the normal \mathbf{n}^{a-a} to line $a-a$ at each point on line $a-a$, we get

$$\int_{a-a} \mathbf{t}^{a-a}(P) \cdot \mathbf{n}^{a-a} dS = 0. \tag{2.26}$$

On the other hand, by accounting for the fact that along line $a-a$, the stress vectors $\mathbf{t}^{a-a}(P)$ must satisfy condition (2.25), from condition (2.26) we obtain

$$\mathbf{t}^{(\mathbf{n}^{a-a})}(P) \cdot \hat{\mathbf{n}}^{a-a}(P) = 0, \tag{2.26'}$$

whence, if

$$\mathbf{t}^{(\mathbf{n}^{a-a})}(P) \neq 0, \tag{2.27}$$

at each point P on the line $a-a$, a distribution of shear stresses could develop along the edge $a-a$. This is however inadmissible, because a positive principal stress could occur along the line $a-a$, which contrasts with (2.24). Consequently, the stress states along $a-a$ is *null*, that is

$$\mathbf{t}^{(\mathbf{n}^{a-a})}(P) = 0. \tag{2.27'}$$

This also occurs along any section $b-b$ transverse to the considered band, as well as along any inclined section $c-c$ in Fig. 2.20. The side bands of the considered masonry are thus unloaded.

In Chap. 6 it will be shown that the lack of loads dispersion actually occurs in masonry walls. This result does not imply that there cannot exist stress distributions radiating from a point of a solid, related to the peculiar load distribution on the surface of the body. The rightmost scheme in Fig. 2.24 shows such a case.

Masonry *channels* the applied loads within its interior to its boundaries along well-defined compression bands determined by the loads' geometry. *The loads determine the resistant masonry structure within the actual masonry body: If the loads change, the resistant masonry structure will consequently change.* Viollet–Le Duc (1854–1868) clearly grasped this peculiar behavior of masonry constructions.

The behavior of linear elastic bodies is completely different, in that such bodies, to the contrary, spread out the action of point loads and, according to the so-called St. Venant principle, ‘soften’ the actions of self-equilibrated load distributions.

2.4.4 *Impenetrability Condition on the Displacement Fields*

The strains and detachments that can occur in a masonry body are defined by displacement fields

$$\mathbf{u}(P), P \in \Omega, \quad (2.28)$$

called *mechanisms*, where Ω is the region occupied by the body of boundary $\partial\Omega$, which we assume to be sufficiently regular. These displacement functions must satisfy suitable *kinematic compatibility conditions*, which we shall now examine. *Impenetrability* between the rigid stones requires that the displacement function $\mathbf{u}(P)$ cannot produce any contraction between points connected by segments *entirely contained within the body*. Thus, if (P_1, P_2) is such a pair of points in Ω , and (Q_1, Q_2) is the corresponding pair after the transformation

$$d(Q_1, Q_2) \geq d(P_1, P_2) \quad (2.29)$$

where $d(Q_1, Q_2)$ denotes the distance of the segment connecting the points (Como 1992). According to these assumptions, *no internal sliding can occur*. Consequently during the development of body deformation, cracks or detachments, representing point discontinuities of the displacement function $\mathbf{u}(P)$, must represent *openings*. In short, masonry material can only *expand or be opened*. Thus, the relative displacement between a pair of points located across the line of the crack will occur along the direction *normal* to the crack.

2.4.5 *Compatibility Conditions on Strains and Detachments*

Let us consider the line f of the crack and its two edges f^- and f^+ (Fig. 2.25). We choose a point P on f and the corresponding points P^- on edge f^- and P^+ on the other edge f^+ , obtained by intersecting f^- and f^+ with the line of the unit vector, for instance \mathbf{n}^- , located along the outward normal to f^- and passing through P^-

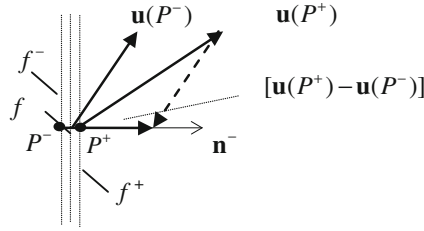


Fig. 2.25 The opening of a crack

(Fig. 2.25). Cracks can *open* only along the direction of \mathbf{n}^- . We can thus define the *crack opening vector* or the *detachment vector* as follows:

$$\Delta^{(n^-)}\mathbf{u}(P) = [u(P^+) - u(P^-)]\mathbf{n}^-, \tag{2.30}$$

whence we obtain

$$[\mathbf{u}(P^+) - \mathbf{u}(P^-)] \cdot \mathbf{n}^- = u(P^+) - u(P^-) > 0, \tag{2.31}$$

where $u(P^+)$ and $u(P^-)$ are the scalar values of $\mathbf{u}(P^+)$ and $\mathbf{u}(P^-)$. Consequently, we can define the scalar *crack opening* by means of the *positive* quantity

$$\Delta^{(n^-)}u(P) = u(P^+) - u(P^-) > 0. \tag{2.32}$$

Inequality (2.32) is the first kinematic compatibility condition to be satisfied by the mechanism displacement $\mathbf{u}(P)$ along the cracks (Como 1992).

Strains, expressed by mean derivatives of function $\mathbf{u}(P)$, can conversely develop within those regions of the masonry body where the displacement function $\mathbf{u}(P)$ is sufficiently regular. These strains can only involve expansions, and so at each point of these regions we have the condition

$$\boldsymbol{\varepsilon}(P) \geq 0, \tag{2.33}$$

which signifies simply that the smallest of the principal strains cannot be negative. The set of all strain tensors satisfying the inequality (2.33) is denoted by Y' . Lastly, the presence of external constraints along boundary $\partial\Omega$ of the body requires further restrictions to the displacement fields.

Let $\partial\Omega_r$ be the part of the surface of the body where restraints are applied and \mathbf{n} be the outward normal at the any given point P of $\partial\Omega_r$. During deformation parts of the body's boundary can *detach* from the surface $\partial\Omega_r$, initially in contact with the body. Thus, if \mathbf{n} is the outward normal to $\partial\Omega_r$, the following condition will hold (Fig. 2.26)

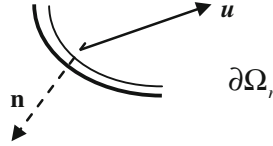


Fig. 2.26 Unilateral boundary constraint of the masonry body

$$\mathbf{u}(P) \cdot \mathbf{n} \leq 0, \quad \forall P \in \partial\Omega_r. \quad (2.34)$$

Inequalities (2.32–2.34) represent the kinematic compatibility conditions imposed on displacement functions $\mathbf{u}(P)$. In particular, inequalities (2.32) and (2.33) must be satisfied on the sets of points defined by the displacement field $\mathbf{u}(P)$ itself. Redefinition of the boundary and interior of the cracked masonry body is required and will be addressed in the following.

2.4.6 The Boundary of the Cracked Body

Developing a general analysis of the equilibrium of masonry bodies is generally a very difficult task due to the discontinuities present in the corresponding displacement functions. Volpert and Hujiajev's idea (1985) of including the set of all discontinuity points of the function $\mathbf{u}(P)$ within the body's boundary turns out to be quite fruitful. First of all, the previous conditions on stress and strain and on stress vectors and detachments. Following this suggestion and Como's formulations (1992), let us now consider, for any displacement field $\mathbf{u}(P)$ of the masonry body satisfying all previous compatibility conditions, the set

$$\Gamma(\mathbf{u}) \quad (2.35)$$

of all points of discontinuities, that is, the set of all cracks, *each with its two edges*. This set is a new part of the boundary of the body, generated by the cracks associated to mechanism $\mathbf{u}(P)$. Consequently, we can define, the region $\Omega(\mathbf{u})$ lacking cracks associated to mechanism $\mathbf{u}(P)$, that is, the region

$$\Omega(\mathbf{u}) = \Omega / \Gamma(\mathbf{u}). \quad (2.36)$$

As per customary representations, the left-hand scheme in Fig. 2.27 shows the boundary of the masonry body crossed by crack f ; the right-hand scheme instead shows the boundary $\partial\Omega(\mathbf{u})$ that includes the two edges of crack f . This latter shows that we can cover the entire boundary $\partial\Omega(\mathbf{u})$, for instance, by circling region $\Omega(\mathbf{u})$ in the counter clockwise direction, that is, having region $\Omega(\mathbf{u})$ always on the left. The kinematic compatibility conditions (2.32–2.34) can now be more thoroughly specified. Thus, following (2.32) and (2.33), the following conditions hold

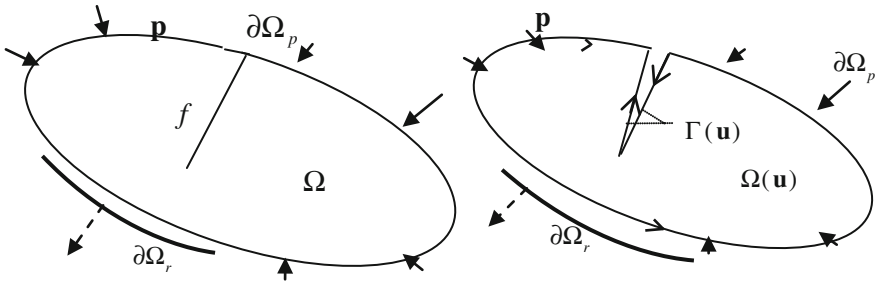


Fig. 2.27 The boundary of the masonry body and the new boundary of the cracked body corresponding to mechanism \mathbf{u}

$$\Delta^{(n^-)}u(P) = u(P^+) - u(P^-) > 0 \quad P \in \Gamma(\mathbf{u}) \tag{2.37}$$

$$\varepsilon(P) \geq 0 \quad P \in \Omega(\mathbf{u}). \tag{2.37'}$$

The first is defined along the cracks, i.e. on the region $\Gamma(\mathbf{u})$ and the second in the region $\Omega(\mathbf{u})$, free from cracks.

Let us consider now the stress vector along a crack, i.e. on the region $\Gamma(\mathbf{u})$ at the actual stress state of the cracked body.

Recalling the previous definition of crack orientation, let us reconsider line f of the crack having two edges f^- and f^+ and the two points P^- and P^+ located respectively along the edges f^+ and f^- . The orientation of the crack is defined by the unit vector \mathbf{n}^- of the outward normal to f^- passing through P^- (Fig. 2.28). The *actual* tension vector

$$\mathbf{t}_a^{(n^-)}(P^-) \tag{2.38}$$

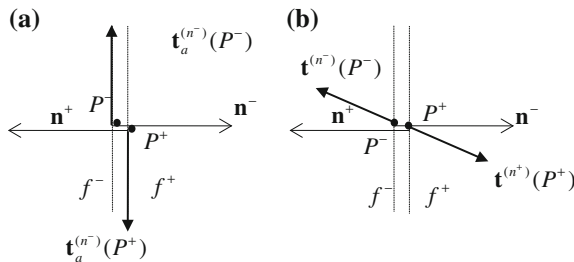


Fig. 2.28 **a** Actual stress vector, not admissible unless null. **b** Generic stress vector acting on the crack edge

cannot thrust on the *actual* crack edge. Thus, we have

$$\mathbf{t}_a^{(n^-)}(P^-) \cdot \mathbf{n}^- = 0, \quad P^- \in f^-. \quad (2.39)$$

Likewise, considering the opposite tension vector,

$$\mathbf{t}_a^{(n^+)}(P^+) \quad (2.38')$$

applied at P^+ on the opposite edge f^+ of the crack, equal and opposite to $\mathbf{t}_a^{(n^-)}(P^-)$, such that

$$\mathbf{t}_a^{(n^+)}(P^+) = -\mathbf{t}_a^{(n^-)}(P^-), \quad (2.40)$$

will satisfy the condition

$$\mathbf{t}_a^{(n^+)}(P^+) \cdot \mathbf{n}^+ = 0, \quad P \in f^+ \quad (2.39')$$

Consequently, if not equal to zero, $\mathbf{t}_a^{(n^-)}(P^-)$, will be orthogonal to \mathbf{n}^- to edge f^- and $\mathbf{t}_a^{(n^+)}(P^+)$ will be orthogonal to the normal \mathbf{n}^+ to edge f^+ . But shearing stresses cannot be exist along the crack edges f^- and f^+ , as shown at Sect. 2.3.3. Consequently, the stress vector is *null* along the crack edges and *no stress transmission* occurs across the cracks at the actual state of the masonry body. Thus we have

$$\mathbf{t}_a^{(n^-)}(P^-) = 0, \quad P^- \in f^- \quad \mathbf{t}_a^{(n^+)}(P^+) = 0, \quad P \in f^+ \quad (2.41)$$

Likewise, if we consider, in place of the actual tension vector acting along the crack, *any admissible* tension vector $\mathbf{t}_a^{(n^-)}(P^-)$ applied at P^- , or $\mathbf{t}_a^{(n^+)}(P^+)$ applied at P^+ , we can write

$$\mathbf{t}_a^{(n^-)}(P^-) \cdot \mathbf{n}^- \leq 0, \quad P^- \in f^- \quad \mathbf{t}_a^{(n^+)}(P^+) \cdot \mathbf{n}^+ \leq 0, \quad P^+ \in f^+. \quad (2.42)$$

2.4.7 *Coupled Conditions on Stresses and Strains and on Stress Vectors and Detachments*

Within the region lacking cracks $\Omega(\mathbf{u})$ only purely stretching strains can occur. These can effectively develop at each point $P \in \Omega(\mathbf{u})$ and along a given direction only if the actual stress component at P and along the same direction vanishes. In brief, extensions can occur only in the directions along which the compressive stress is zero. Thus, the following normality condition holds (Fig. 2.29)

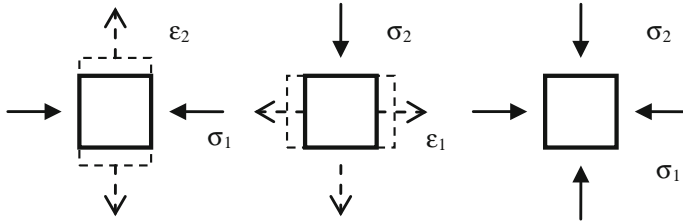


Fig. 2.29 Admissible stresses and strains in masonry material

$$\sigma_a(P) \cdot \varepsilon(P) = 0 \quad P \in \Omega(\mathbf{u}), \tag{2.43}$$

where $\sigma_a(P)$ is the *actual* stress and $\varepsilon(P)$ the *actual* strain at P . It is worth pointing out that condition (2.43) extends to the continuum the simple, intuitive condition (2.15) discussed for the unit resistant masonry cell.

Likewise, as consequence of (2.24) and (2.33), the *generic* admissible stress and the generic admissible strain at a point P of region $\Omega(\mathbf{u})$ will be linked by the following inequality

$$\sigma(P) \cdot \varepsilon(P) \leq 0 \quad P \in \Omega(\mathbf{u}) \quad \forall \sigma \in Y, \forall \varepsilon \in Y'. \tag{2.44}$$

Equivalent relations hold along the cracks. By coupling the conditions involving generic admissible stress vectors and detachments, we can immediately establish the following inequalities

$$\mathbf{t}_a^{(n^-)}(P^-) \cdot \Delta^{(n^-)}\mathbf{u}(P) \leq 0, \quad \mathbf{u} \in M, P \in f^- \tag{2.45}$$

or,

$$\mathbf{t}_a^{(n^+)}(P^+) \cdot \Delta^{(n^+)}\mathbf{u}(P) \geq 0, \quad \mathbf{u} \in M, P \in f^+, \tag{2.45'}$$

which must be satisfied by *any* admissible stress vector $\mathbf{t}^{(n)}(P)$ and admissible detachment $\Delta^{(n)}(P)\mathbf{u}$. Conditions (2.45) and (2.45') show that the admissible stress vectors, cannot never *pull* within the interior of the body.

2.4.8 Specifications for One-Dimensional Masonry Systems

The previous general definitions can be specified for the simple case of one-dimensional structures, as, for instance, for a masonry arch.

Let us consider, for instance, the arch illustrated in Fig. 2.30, whose pressure line, wholly within the arch, meets the arch extrados at points A and C and its intrados at B and D. Hinges are thus formed at A, B, C and D. A mechanism displacement ensues. The corresponding vertical displacements of the arch are

Fig. 2.30 The pressure line of the arch

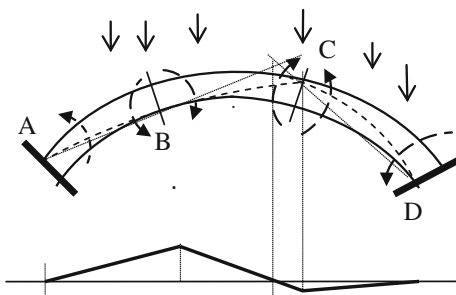
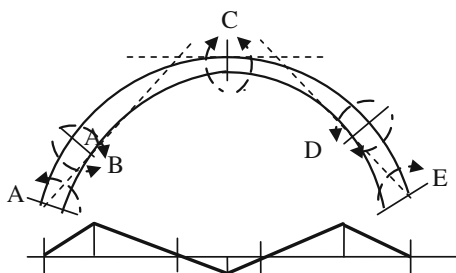


Fig. 2.31 Symmetric five-hinge mechanism in an arch



shown in Fig. 2.30. The mechanism is kinematically compatible. In fact, the counter clockwise rotation at hinge A of segment AB detaches section A from the left springing of the arch; likewise, the rotation of CD at D, also counter clockwise, detaches section D from the right springing. Relative rotations at B and C occur with the formation of opening hinges at B and C. Figure 2.31 shows a symmetric mechanism composed of the four rigid segments AB, BC, CD and DE connected by the five hinges A, B, C, D and E. The relative rotations occurring between contiguous rigid segments give rise to compatible deformations.

Lastly, Fig. 2.32 shows two mechanisms, the left compatible, the right incompatible.

2.4.9 Indeformable Masonry Structures

Due to their geometries and constraints some masonry structures cannot be deformed to give rise to mechanisms: interpenetration of the material arises for any hinge position. Examples of structures of this type are the flying buttress or the platbands inserted between fixed springers (Fig. 2.33, left and middle). For such structural systems, in short, we have

$$M = \emptyset. \tag{2.46}$$

This condition is a consequence of the assumption of the compressionally rigid material. Another example is the stair ramp shown at the left in Fig. 2.33.

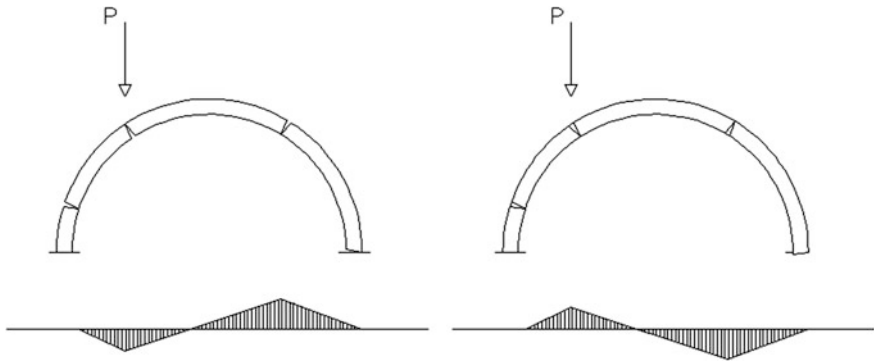


Fig. 2.32 Compatible mech. Incompatible mech

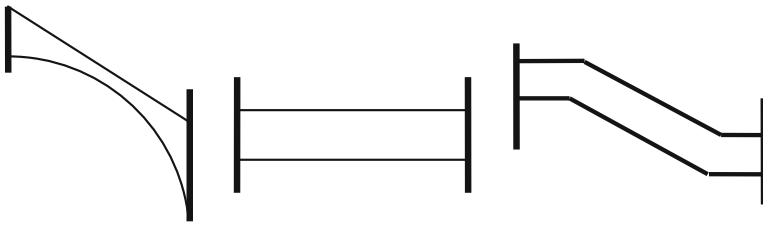


Fig. 2.33 Examples of no mechanisms masonry structures

2.5 Equilibrium and Compatibility

2.5.1 Principle of Virtual Work

Let us consider a masonry body under the action of the loads \mathbf{p} at an admissible equilibrium state. Let $\delta\mathbf{u}(P) \in M$ be a mechanism field, representing a kinematically admissible virtual displacement of the body. Cracks will arise during the development of the virtual mechanism $\delta\mathbf{u}(P)$ and $\Gamma(\delta\mathbf{u})$ will be the region representing the cracks' boundaries. Consequently,

$$\Omega(\delta\mathbf{u}) = \Omega / \Gamma(\delta\mathbf{u}) \tag{2.47}$$

is the corresponding region occupied by the *crack-free* body. The new boundary of the body associated to the virtual displacement $\delta\mathbf{u}$ is then obtained by adding to the initial boundary $\partial\Omega$ the crack boundaries, that is,

$$\partial\Omega(\delta\mathbf{u}) = \partial\Omega \cup \Gamma(\delta\mathbf{u}). \tag{2.48}$$

The virtual displacement $\delta \mathbf{u}$ satisfies the above kinematic compatibility conditions along the discontinuities' surfaces $\Gamma(\delta \mathbf{u})$ and we thus have

$$\Delta^{(n^-)} \delta u(P) = \delta u(P^+) - \delta u(P^-) > 0 \quad P \in \Gamma(\delta \mathbf{u}). \quad (2.49)$$

Moreover, in the inner crack-free region $\Omega(\delta \mathbf{u})$, the corresponding strains, in conformity with (2.33), will satisfy the following inequality

$$\delta \boldsymbol{\varepsilon}(P) \geq 0, \quad \delta \boldsymbol{\varepsilon} = D \delta \mathbf{u}(P), \quad P \in \Omega(\delta \mathbf{u}), \quad (2.50)$$

where D is the known operator that associates the strains $\delta \boldsymbol{\varepsilon}$ to the displacement $\delta \mathbf{u}$ in $\Omega(\delta \mathbf{u})$. Finally, according to conditions (2.34), on the boundary $\partial \Omega_r$ we have

$$\delta \mathbf{u}(P) \cdot \mathbf{n} \leq 0, \quad P \in \partial \Omega_r \quad (2.51)$$

The virtual mechanism $\delta \mathbf{u}$ will satisfy the *kinematic compatibility* conditions (2.49–2.51). Likewise, we can define the *static compatibility* conditions for the admissible stresses in equilibrium with loads \mathbf{p} . Thus, from (2.44) we have

$$\boldsymbol{\sigma}(P) \cdot \delta \boldsymbol{\varepsilon}(P) \leq 0, \quad \delta \boldsymbol{\varepsilon}(P) = D \delta \mathbf{u}(P), \quad P \in \Omega(\delta \mathbf{u}), \quad \delta \mathbf{u} \in M. \quad (2.52)$$

At the same time, considering the two points P^- and P^+ located along the direction of the outward normal to a virtual crack, where the jump $\Delta^{(n^-)} \mathbf{u}(P^-)$ of $\delta \mathbf{u}(P)$ occurs, from (2.45) we have

$$\mathbf{t}^{(n^+)}(P^+) \cdot \Delta^{(n^-)}(P^-) \delta \mathbf{u} \geq 0, \quad \delta \mathbf{u} \in M, \quad P \in f^+. \quad (2.53)$$

Lastly, the reaction \mathbf{r} , acting along $\partial \Omega_r$, will satisfy the condition

$$\mathbf{r}(P) \cdot \delta \mathbf{u}(P) \geq 0, \quad P \in \partial \Omega_r. \quad (2.54)$$

Inequalities (2.52–2.54) are the coupled compatibility conditions associated to the virtual mechanism $\delta \mathbf{u}(P)$. These conditions, together with the internal equilibrium equations, define the admissible equilibrium state of the masonry solid, which, for the sake of simplicity, we will indicate as AE.

The equilibrium of the body is governed by the principle of the so called *virtual works* or of the *virtual displacements*. This principle will take a *particular form* that is representative of the compressionally rigid no-tension bodies that will be analyzed along the lines previously set forth by Como (1992, 2012). At any point P within the region $\Omega(\delta \mathbf{u})$, the stress field $\boldsymbol{\sigma}$ will satisfy inequality (2.52) together with the following internal equilibrium equation

$$\sigma_{ij,j} + \rho_i = 0. \quad (2.55)$$

Now let dV be a generic volume element around P in $\Omega(\delta \mathbf{u})$. The virtual work done to displace this element is

$$(\sigma_{ij,j} + \rho_i)\delta u_i dV. \tag{2.56}$$

According to the equilibrium Eq. (2.55), this work vanishes. Integration of (2.56) over the volume $\Omega(\delta\mathbf{u})$ thus yields

$$\int_{\Omega(\delta\mathbf{u})} (\sigma_{ij,j} + \rho_i)\delta u_i dV = 0. \tag{2.57}$$

From (2.57), the Gauss–Green theorem, together with some tensor calculations and previous specifications, enables us to obtain

$$\int_{\Omega(\delta\mathbf{u})} \sigma_{ij,j}\delta\varepsilon_{ij}dV = \int_{\partial\Omega(\delta\mathbf{u})} t_i^{(\mathbf{n})}\delta u_i dS + \int_{\Omega(\delta\mathbf{u})} \rho_i\delta u_i dV, \tag{2.58}$$

where \mathbf{n} is the unit vector along the outward normal to the crack surface.

Figure 2.34a shows a masonry arch in an admissible equilibrium state under the action of loads \mathbf{p} and internal stress $\boldsymbol{\sigma}$. Figure 2.34b also shows the displacement field $\delta\mathbf{u}$ with hinges A, B, C and D, together with the corresponding internal cracks BB' and CC' . Figure 2.34a, b also show:

- the cracks’ boundaries $\Gamma(\delta\mathbf{u})$;
- the region $\Omega(\delta\mathbf{u}) = \Omega/\Gamma(\delta\mathbf{u})$ lacking cracks;
- the overall boundary of the body, including the crack boundaries $\partial\Omega(\delta\mathbf{u}) = \partial\Omega \cup \Gamma(\delta\mathbf{u})$.

The entire boundary can also be specified by the union of the boundaries $\Gamma(\delta\mathbf{u})$, $\partial\Omega_r$ and $\partial\Omega_p$,

$$\partial\Omega(\delta\mathbf{u}) = \Gamma(\delta\mathbf{u}) \cup \partial\Omega_r \cup \partial\Omega_p. \tag{2.59}$$

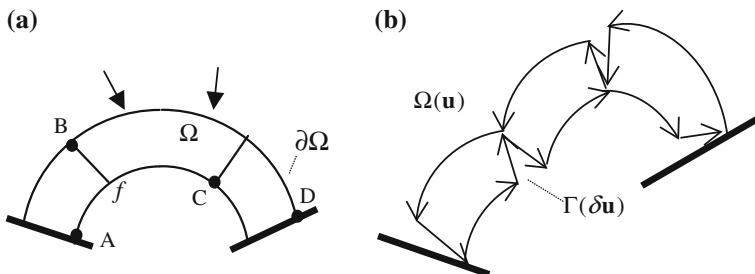


Fig. 2.34 The boundary of the crack-free arch and the new boundary including the cracks associated to virtual mechanism $\delta\mathbf{u}$

The internal work (2.58) can now be written in a more explicit form. In fact, according to (2.59), we have

$$\int_{\Omega(\delta u)} \sigma_{ij,j} \delta \varepsilon_{ij} dV = \int_{\Gamma(\delta u)} t_i^{(n)} \delta u_i dS + \int_{\partial \Omega_e} r_i^{(n)} \delta u_i dS + \int_{\partial \Omega_p} p_i^{(n)} \delta u_i dS + \int_{\Omega(\delta u)} \rho_i \delta u_i dV. \quad (2.60)$$

To work out the first integral in the second member of (2.60), by moving around the whole contour of the body, the virtual work of the interactions $t_i^{(n)}$ can be evaluated along each of the two edges of the cracks (Fig. 2.34b). For the sake of simplicity, we can refer to a single crack alone and write

$$\Gamma(\delta u) = \Gamma_1(\delta u) \cup \Gamma_2(\delta u), \quad (2.61)$$

where $\Gamma_1(\delta u)$ and $\Gamma_2(\delta u)$ are the two equal surfaces representing the two edges of the crack. Evaluating the first integral in the second member of (2.60) thus gives

$$\int_{\Gamma(\delta u)} t_i^{(n)} \delta u_i dS = \int_{\Gamma_1(\delta u)} t_i^{(n^-)} \delta u_i(P^-) dS + \int_{\Gamma_2(\delta u)} t_i^{(n^+)} \delta u_i(P^+) dS. \quad (2.62)$$

On the other hand, using expression (2.32) for the crack opening $\Delta^{(n^-)} u(P)$, we have

$$\delta u_i(P^-) = \delta u_i(P^+) - \Delta^{(n^-)} \delta u_i(P); \quad (2.63)$$

Substituting (2.63) into (2.62) gives

$$\begin{aligned} \int_{\Gamma(\delta u)} t_i^{(n)} \delta u_i dS &= \int_{\Gamma_1(\delta u)} t_i^{(n^-)} \delta u_i(P^+) dS \\ &- \int_{\Gamma_1(\delta u)} t_i^{(n^-)} \Delta^{(n^-)} \delta u_i(P) dS + \int_{\Gamma_2(\delta u)} t_i^{(n^+)} \delta u_i(P^+) dS. \end{aligned} \quad (2.62')$$

Furthermore, by taking into account that

$$t_i^{(n^-)} = -t_i^{(n^+)}, \quad (2.64)$$

we get

$$\int_{\Gamma(\delta\mathbf{u})} t_i^{(\mathbf{n})} \delta u_i dS = - \int_{\Gamma_1(\delta\mathbf{u})} t_i^{(\mathbf{n}^+)} \delta u_i (P^+) dS - \int_{\Gamma_2(\delta\mathbf{u})} t_i^{(\mathbf{n}^-)} \Delta^{(n^-)} \delta u_i (P) dS + \int_{\Gamma_2(\delta\mathbf{u})} t_i^{(\mathbf{n}^+)} \delta u_i (P^+) dS. \quad (2.62')$$

On the other hand,

$$\int_{\Gamma_1(\delta\mathbf{u})} t_i^{(\mathbf{n}^+)} \delta u_i (P^+) dS = \int_{\Gamma_2(\delta\mathbf{u})} t_i^{(\mathbf{n}^+)} \delta u_i (P^+) dS. \quad (2.65)$$

In fact, the integral is evaluated on the same surface because $\Gamma_1(\delta\mathbf{u})$ and $\Gamma_2(\delta\mathbf{u})$ are equal, hence

$$\int_{\Gamma(\delta\mathbf{u})} t_i^{(\mathbf{n})} \delta u_i dS = - \int_{\Gamma_2(\delta\mathbf{u})} t_i^{(\mathbf{n}^-)} \Delta^{(n^-)} \delta u_i \quad (2.66)$$

or

$$\int_{\Gamma(\delta\mathbf{u})} t_i^{(\mathbf{n})} \delta u_i dS = \int_{\Gamma_1(\delta\mathbf{u})} t_i^{(\mathbf{n}^+)} \Delta^{(n^-)} \delta u_i dS \quad (2.66')$$

Finally, summing up the work along all the crack surfaces, we get

$$\int_{\Omega(\delta\mathbf{u})} \sigma_{ijj} \delta \varepsilon_{ij} dV = \sum_k \int_{\Gamma_k^+(\delta\mathbf{u})} t_i^{(\mathbf{n}^+)} \Delta^{(n^-)} \delta u_i dS + \int_{\partial\Omega} r_i^{(\mathbf{n})} \delta u_i dS + \int_{\partial\Omega_p} p_i^{(\mathbf{n})} \delta u_i dS + \int_{\Omega(\delta\mathbf{u})} \rho_i \delta u_i dV. \quad (2.67)$$

With the following definitions

$$\{\mathbf{t}^{(\mathbf{n}^+)}, \Delta^{(n^-)} \delta \mathbf{u}\} = \sum_k \int_{\Gamma_k^+(\delta\mathbf{u})} t_i^{(\mathbf{n}^+)} \Delta^{(n^-)} \delta u_i dS \quad \langle \mathbf{r}, \delta \mathbf{u} \rangle = \int_{\partial\Omega} r_i^{(\mathbf{n})} \delta u_i dS; \quad (2.68)$$

$$\langle \mathbf{p}, \delta \mathbf{u} \rangle = \int_{\partial\Omega_p} p_i^{(\mathbf{n})} \delta u_i dS + \int_{\Omega(\delta\mathbf{u})} \rho_i \delta u_i dV; \quad \langle \boldsymbol{\sigma}, \delta \boldsymbol{\varepsilon} \rangle = \int_{\Omega(\delta\mathbf{u})} \sigma_{ijj} \delta \varepsilon_{ij} dV, \quad (2.68')$$

condition (2.67) becomes

$$\langle \boldsymbol{\sigma}, \delta \boldsymbol{\varepsilon} \rangle = \{ \mathbf{t}^{(n^+)}, \Delta^{(n^-)} \delta \mathbf{u} \} + \langle \mathbf{r}, \delta \mathbf{u} \rangle + \langle \mathbf{p}, \delta \mathbf{u} \rangle \quad \forall \delta \mathbf{u} \in M. \quad (2.69)$$

Moreover, inequalities (2.52), (2.53) and (2.54) can be expressed as

$$\langle \boldsymbol{\sigma}, \delta \boldsymbol{\varepsilon} \rangle \leq 0 \quad \{ \mathbf{t}^{(n^+)}, \Delta^{(n^-)} \delta \mathbf{u} \} \geq 0 \quad \langle \mathbf{r}, \delta \mathbf{u} \rangle \geq 0. \quad (2.70)$$

Vice versa, working back step by step from Eq. (2.69), we arrive at Eq. (2.55), of course, in obedience of all compatibility conditions.

Thus, conditions (2.69) and (2.70) are *necessary and sufficient* for the admissible equilibrium and provide a suitable representation for the principle of virtual work for rigid no-tension masonry bodies (Como 1992). Comparing the current formulation of the same principle for linear elastic solids with this one concerning no-tension bodies, the difference is that here the work of the tension vectors of the virtual detachments $\Delta \delta \mathbf{u}$ must be added, as must also the associated compatibility conditions (2.70). Figure 2.41 shows the two systems, of forces and deformations, respectively statically and kinematically compatible, connected together by condition (2.69), representing the principle of virtual works.

2.5.2 Variational Inequality for the Existence of the Admissible Equilibrium State

A correctly constrained linear elastic structure is always able to reach a consistent, equilibrated configuration. In brief, the problem of the linear elastic equilibrium admits a solution for any loads distribution. However, for no-tension masonry structures this no longer holds true. Masonry structures can, on the contrary, collapse under loading \mathbf{p} . It is therefore useful to seek conditions, involving only *known* quantities, that enable predicting whether any given body made of a rigid no-tension material can withstand the action of the assigned loads. Although conditions (2.69) and (2.70) are necessary and sufficient to guarantee the existence of admissible equilibrium, they must be satisfied by both the loads and the internal stresses. However, these latter may be a priori unknown.

In this section we shall prove that the variational inequality on loads \mathbf{p} alone

$$\langle \mathbf{p}, \delta \mathbf{u} \rangle \leq 0, \quad \forall \delta \mathbf{u} \in M \quad (2.71)$$

is *necessary and sufficient* to guarantee the existence of the AE state.

It should be noted that the mechanisms $\delta \mathbf{u}$ represent the various deformation modes of the body. Inequality (2.71) thus simply means that the body is in an AE state under loads \mathbf{p} *iff* the work of these loads \mathbf{p} is *not positive* along any possible deformation of the body.

Necessity follows immediately from (2.69) and (2.70). In the context of elastic no-tension models, proofs of the sufficiency of condition (2.71) have been furnished by Romano and Romano (1985) and Romano and Sacco (1986). Another simple proof, in the framework of the rigid no-tension model, has been given by Como (1992). The main lines of this latter proof are the following.

If the variational inequality (2.71) was only necessary, but insufficient, it could be also satisfied by loads \mathbf{p} unsustainable by the body in the AE state. Such a situation is however impossible. It will in fact be shown that any load \mathbf{p} that is unsustainable by the body in an AE state and that consequently sets the body in motion (Fig. 2.35), does *positive* work on displacement \mathbf{v} along which the body begins to move. This contradiction with the assumption proves the statement.

Let us therefore assume, *ad absurdum*, that, in spite of condition (2.71), the body is *not* in an AE state under loads \mathbf{p} , and let us then consider the motion defined by the velocity field $\mathbf{v}(P, t)$ initiated just after application of the loads. A simple example is represented by the collapse of an arch loaded by its weight and a central point load, as in Fig. 2.36. The body will begin to move. At any instant during the motion, the stress field $\boldsymbol{\sigma}$ will satisfy the internal constraints, i.e., condition (2.24), and the normality rule (2.43). Thus,

$$\boldsymbol{\sigma}(P, t) \leq 0, \quad \boldsymbol{\sigma}(P, t) \cdot \underline{\boldsymbol{\varepsilon}}(P, t) = 0, \quad P \in \Omega(\mathbf{v}), \quad \forall t \geq 0. \quad (2.72)$$

By applying the virtual work equation in which we take, as virtual displacement $\delta \mathbf{u}$, the actual displacement occurring during movement of the body over time interval dt , we have

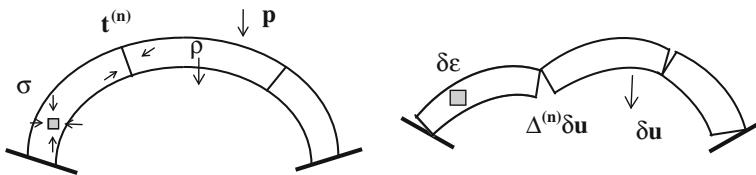
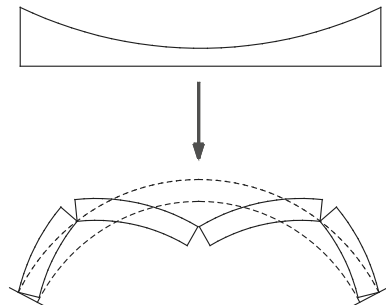


Fig. 2.35 The two systems, forces and deformations, respectively statically and kinematically compatible, connected by the virtual work equation

Fig. 2.36 The masonry arch at incipient failure



$$\delta \mathbf{u} = \mathbf{v}(P, t) dt. \quad (2.73)$$

Thus, with

$$\delta \boldsymbol{\varepsilon} = \boldsymbol{\varepsilon}(P, t) dt, \quad \Delta^{(n)} \delta \mathbf{u} = \Delta^{(n)} \mathbf{v}(P, t) dt \quad (2.73')$$

where $\dot{\varepsilon} = d\varepsilon/dt$ and taking into account the inertial forces produced in the body due to acceleration $\dot{\mathbf{v}}$, we obtain

$$\langle \boldsymbol{\sigma}, \dot{\varepsilon} \rangle = \{ \mathbf{t}^{(n^+)}, \Delta^{(n^-)} \mathbf{v} \} + \langle \mathbf{r}, \mathbf{v} \rangle + \langle \mathbf{p}, \mathbf{v} \rangle - \langle \rho \dot{\mathbf{v}}, \mathbf{v} \rangle, \quad t > 0. \quad (2.74)$$

Thus, during the motion we have, with the previous notation,

$$\langle \boldsymbol{\sigma}(P), \dot{\varepsilon} \rangle = 0, \quad \{ \mathbf{t}^{(n^+)}, \Delta^{(n^-)} \mathbf{v} \} = 0 \quad \langle \mathbf{r}, \mathbf{v} \rangle = 0. \quad (2.75)$$

The first of conditions (2.75) follows from the second of (2.72). Regarding the second condition, note that when cracks begin to open, the stress interaction $\mathbf{t}^{(n^+)}$ vanishes since $\Delta^{(n^-)} \mathbf{v} \neq 0$ along them.

Likewise, if during the motion, the body is displaced away from the constraint boundary $\partial\Omega_c$, there $\mathbf{v} \neq 0$ and consequently $\mathbf{r} = 0$, and the last condition in (2.75) also holds. Thus, condition (2.74) becomes

$$\langle \mathbf{p}, \mathbf{v} \rangle - \langle \rho \dot{\mathbf{v}}, \mathbf{v} \rangle = 0, \quad t > 0. \quad (2.76)$$

The kinetic energy of the body is

$$T = 1/2 \langle \rho \mathbf{v}, \mathbf{v} \rangle \quad (2.77)$$

and its rate of change is

$$\frac{dT}{dt} = \langle \rho \dot{\mathbf{v}}, \mathbf{v} \rangle. \quad (2.78)$$

Equation (2.76) thus becomes

$$\langle \mathbf{p}, \mathbf{v} \rangle = \frac{dT}{dt}, \quad t > 0. \quad (2.79)$$

However, when the body begins to move the derivative dT/dt of the kinetic energy can only be positive. Thus, if loads \mathbf{p} are applied and cannot be sustained, the body begins to move and the work done by loads \mathbf{p} along the displacement of this motion is positive. Such a result contradicts assumption (2.71), whence we can conclude that if $\langle \mathbf{p}, \delta \mathbf{u} \rangle \leq 0, \forall \delta \mathbf{u} \in M$, the body is in an AE state.

2.5.3 No-Existence of Self-Equilibrating Stress Fields in Deformable Structures

Within the framework of no-tension models, another typical aspect of the behavior of masonry bodies that can be deformed with mechanisms, is their inability to sustain self-equilibrated stresses. Likewise, the reactions of constraints vanish in the absence of external loads.

The proof of this property follows immediately from application of the principle of virtual work (2.69), together with compatibility conditions (2.70). In fact, with vanishing loads, the following conditions hold

$$\langle \boldsymbol{\sigma}, \delta \boldsymbol{\varepsilon} \rangle = \{ \mathbf{t}^{(n+)}, \Delta^{(n-)} \delta \mathbf{u} \} + \langle \mathbf{r}, \delta \mathbf{u} \rangle \quad \forall \delta \mathbf{u} \in M; \tag{2.69'}$$

$$\langle \boldsymbol{\sigma}, \delta \boldsymbol{\varepsilon} \rangle \leq 0 \quad \{ \mathbf{t}^{(n+)}, \Delta^{(n-)} \delta \mathbf{u} \} \geq 0 \quad \langle \mathbf{r}, \delta \mathbf{u} \rangle \geq 0 \quad \forall \delta \mathbf{u} \in M. \tag{2.70'}$$

Both conditions (2.69') and (2.70') can be satisfied, $\forall \delta \mathbf{u} \in M$, only if

$$\langle \boldsymbol{\sigma}, \delta \boldsymbol{\varepsilon} \rangle = 0 \{ \mathbf{t}^{(n+)}, \Delta^{(n-)} \delta \mathbf{u} \} = 0 \quad \langle \mathbf{r}, \delta \mathbf{u} \rangle = 0. \tag{2.80}$$

We can now assume that any straight segment S leaving from any point of the *constrained* boundary $\partial\Omega_r$, intersects the opposite side of the body only at points of its *free* boundary, as certainly it turns out for all the structures rising from the ground (Fig. 2.37). Extensions can thus develop along the segments S .

For any point P along S . It will be thus possible to choose a mechanism $\delta \mathbf{u}$ such that in a neighborhood $I(P)$ of P the strains $\boldsymbol{\varepsilon}(\delta \mathbf{u})$ along S will be positive. Consequently, by virtue of (2.80), $\boldsymbol{\sigma} \equiv 0$ in $I(P)$. We can repeat the argument for any other point on S so that $\boldsymbol{\sigma} \equiv 0$ along all the segment S . All the points in the body can be intercepted by segments S and $\boldsymbol{\sigma} \equiv 0$ in the whole body. The same results is obtained considering the occurrence of detachments.

In conclusion, taking into account that conditions (2.80) must be satisfied for each mechanism $\delta \mathbf{u}$, we get

$$\boldsymbol{\sigma} \equiv 0; \quad \mathbf{t}^{(n)} \equiv 0; \quad \mathbf{r} \equiv 0. \tag{2.81}$$

in the *unloaded* masonry structure. Thus, self-stresses and reactions vanish in unloaded masonry structures that can be deformed through mechanisms. Deformable masonry structures can thus be considered *statically determinate systems*.

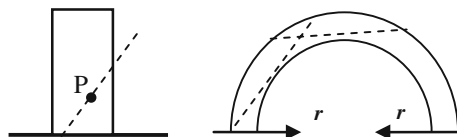


Fig. 2.37 Deformable systems: no self-equilibrated stresses and constraint reactions

2.5.4 *Indeformable Structures: Statically Indeterminate Behaviour*

For indeformable masonry systems the set M of the kinematically admissible mechanisms is empty. Self-equilibrated stresses do exist in indeformable masonry systems. In such cases, conditions (2.80) are in fact satisfied by

$$\delta \boldsymbol{\varepsilon} \equiv 0 \quad \Delta^{(n^-)} \delta \mathbf{u} \equiv 0 \quad \delta \mathbf{u} \equiv 0, \tag{2.82}$$

which, by virtue of (2.80), yields

$$\boldsymbol{\sigma} \neq 0 \quad \mathbf{t}^{(n)} \neq 0 \quad \mathbf{r} \neq 0. \tag{2.83}$$

Figure 2.37 shows some examples of self-stresses acting in indeformable masonry systems. Note that such a state requires the presence of fixed constraints.

The existence of constraint reactions in absence of external loads allows to better define the indeformable structures. For these systems it is in fact possible, starting from a point of the laterally constrained sections, to trace at least one straight line wholly contained within the structure (Fig. 2.38). The flying buttress, sketched in left of Fig. 2.35, is one example of such an indeformable system.

2.5.5 *Admissible Equilibrium in One-Dimensional Systems*

All the foregoing conditions governing the admissible equilibrium of masonry bodies take simpler forms when referred to a one-dimensional structure.

Let us consider the masonry arch shown in Fig. 2.39. It is in an AE state under the action of loads \mathbf{p} . Figure 2.38 shows the pressure line in the arch as the curve joining all points traversed in each section of the arch by the resultant of all the forces preceding or following the section.

The internal stresses, σ , are all compressive in each section of the arch. In one-dimensional systems potential stretching strains of the voussoirs lead to displacements negligible with respect to those produced by the relative rotations at the

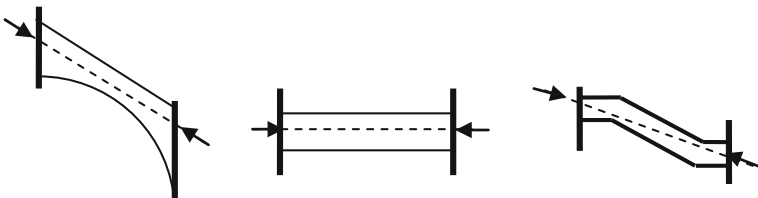


Fig. 2.38 Indeformable systems: existence of self-equilibrated stresses and reactions

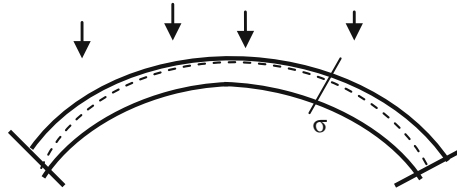


Fig. 2.39 The arch in a statically admissible equilibrium state: the pressure line is wholly contained within the arch

hinges. In defining the corresponding mechanisms, it is thus possible to consider only detachments $\Delta^{(n^-)}\mathbf{u}$ arising in the voussoirs, where hinges develop, and consequently neglect any strains, $\boldsymbol{\varepsilon}$, that may spread into the voussoirs, occupying the region, $\Omega(\mathbf{u})$, defined above.

We can also assume that the external constraints are fixed. Hence, neither the work of reactions, \mathbf{r} , nor the work of stresses, $\boldsymbol{\sigma}$ on the strains, $\boldsymbol{\varepsilon}$, will appear in the virtual work equation. With these restrictions, this equation takes the simpler form

$$\{\mathbf{t}^{(n^+)}, \Delta^{(n^-)}\delta\mathbf{u}\} + \langle \mathbf{p}, \delta\mathbf{u} \rangle = 0 \quad \forall \delta\mathbf{u} \in M, \tag{2.69'}$$

associated to the admissibility condition

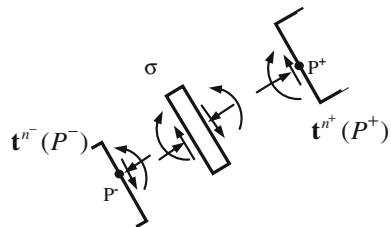
$$\{\mathbf{t}^{(n^+)}, \Delta^{(n^-)}\delta\mathbf{u}\} \geq 0. \tag{2.70'}$$

Recalling previous definitions, note that the symbol in parentheses is the sum of the product of the stress vectors by the corresponding virtual detachments.

The forces acting on the side sections of a small voussoir of the arch are equal and opposite to the resultant of the stress vectors, $\mathbf{t}^{(n^+)}$ and $\mathbf{t}^{(n^-)}$, acting on the sections of the arch facing the side sections of the voussoir.

They can be expressed in terms of the components N , M and T of the resultant vector, $\boldsymbol{\Sigma}$ (Fig. 2.40). Consequently, if, according to (2.45'), the work of $\mathbf{t}^{(n^+)}(P^+)$ on the detachment $\Delta^{(n^-)}\delta\mathbf{u}$ is non-negative, the work of the equal and opposite actions on the detachments themselves will be non-positive (Fig. 2.41).

Fig. 2.40 Internal actions and reactions inside the masonry arch



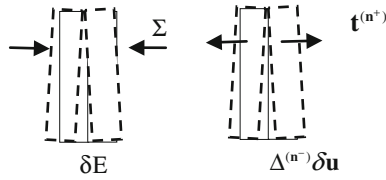


Fig. 2.41 The opposite in sign works of stresses σ and of the stress vectors $\mathbf{t}^{(n+)}$

The resultant of forces $\mathbf{t}^{(n+)}$ or $\mathbf{t}^{(n-)}$ acting on the transverse sections delimiting the crack, where a hinge is formed, can be decomposed into the components of the axial force, N , the bending moment, M , and the shear, T , of the resultant vector Σ , as defined by (2.6). At the same time, the detachments, $\Delta^{(n-)}\delta\mathbf{u}$, can, in turn, be expressed in terms of the virtual deformation vector, $\delta\mathbf{E}$, whose components are the axial displacement, δA , and the relative rotation, $\delta\phi$, defined according to (2.11). In brief, for the sake of simplicity, we can write

$$\{\mathbf{t}^{(n+)}, \Delta^{(n-)}\delta\mathbf{u}\} = -\langle \Sigma, \delta\mathbf{E} \rangle, \tag{2.84}$$

and the equation of virtual work (2.69') becomes

$$\langle \mathbf{p}, \delta\mathbf{u} \rangle = \langle \Sigma, \delta\mathbf{E} \rangle \quad \forall \delta\mathbf{u} \in M, \tag{2.69'}$$

and the admissibility condition on the stresses, finding (2.14), is

$$\langle \Sigma, \delta\mathbf{E} \rangle \leq 0. \tag{2.14'}$$

The virtual work Eq. (2.80) thus takes the typical form expressing the equality between internal and external virtual work (Fig. 2.42).

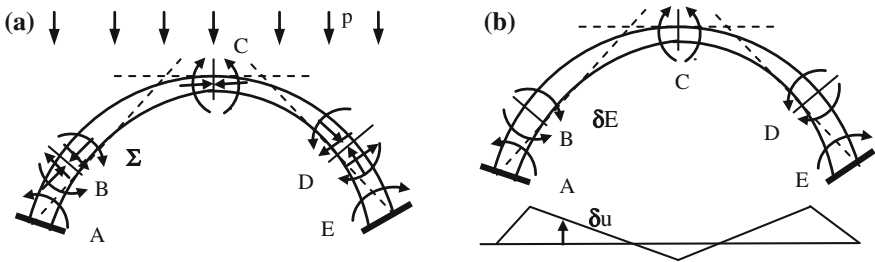


Fig. 2.42 **a** System of external and internal forces. **b** System of virtual displacements and strains

2.5.6 Admissible Equilibrium of Elastic No Tension One-Dimensional Systems

Condition (2.88), with its associated compatibility conditions, can be generalized to the case of structures with *elastic* ashlars free to detach each other (Fig. 2.43).

The virtual strain field can be decomposed into the compressive elastic and the extensive anelastic share

$$E(\delta\mathbf{u}) = E_e(\delta\mathbf{u}) + E_f(\delta\mathbf{u}) \quad \forall \delta\mathbf{u} \in M \tag{2.85}$$

where,

$$E_e(\delta\mathbf{u}) \leq 0; \quad E_f(\delta\mathbf{u}) \geq 0 \quad \forall \delta\mathbf{u} \in M \tag{2.86}$$

Condition (2.69') thus becomes

$$\langle \mathbf{p}, \delta\mathbf{u} \rangle = \langle \Sigma, \mathbf{E}_f(\delta\mathbf{u}) \rangle + \langle \Sigma, \mathbf{E}_e(\delta\mathbf{u}) \rangle \quad \forall \delta\mathbf{u} \in M \tag{2.69'}$$

with

$$\langle \Sigma, \mathbf{E}_e(\delta\mathbf{u}) \rangle \geq 0 \quad \langle \Sigma, \mathbf{E}_f(\delta\mathbf{u}) \rangle \leq 0 \quad \forall \delta\mathbf{u} \in M \tag{2.86'}$$

At the same section at least one of strains $\epsilon_e(\delta\mathbf{u})$ and $\epsilon_f(\delta\mathbf{u})$ is zero. Thus

$$\mathbf{E}_f(\delta\mathbf{u}(P)) \cdot \mathbf{E}_e(\delta\mathbf{u}(P)) = 0 \quad \forall \delta\mathbf{u} \in M \tag{2.87}$$

Using the same argument of Sect. 2.5.3 we can affirm that self stresses cannot develop in the elastic no tension systems, as for the rigid no tension ones.

2.5.7 Weight and Live Loads

Loads acting on a structure can be subdivided into two broad categories having different characteristics. On the one hand, there are the so-called *dead* loads or weight loads \mathbf{g} , which are permanent and generally quite large, and on the other,

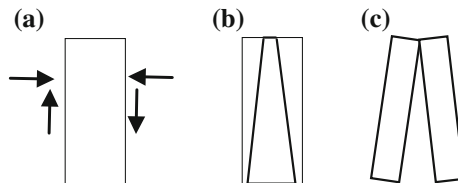


Fig. 2.43 a Admissible Σ . b admissible \mathbf{E}_e . c admissible \mathbf{E}_f

live loads, \mathbf{p} , which can be considered to be determined by the loading parameter λ . Thus, we can write

$$\mathbf{p} = \mathbf{g} + \lambda \mathbf{q}. \tag{2.88}$$

As a rule, the weight, \mathbf{g} , represents the resistant load for a masonry structure. Consequently, recalling condition (2.71), the structure will certainly be *safe* under the action of its own weight \mathbf{g} , and the following condition will be satisfied

$$\langle \mathbf{g}, \mathbf{v} \rangle < 0, \quad \forall \mathbf{v} \in M, \tag{2.71'}$$

or

$$\langle \mathbf{g}, \mathbf{v} \rangle < -k, \quad k > 0, \quad \forall \mathbf{v} \in M. \tag{2.71''}$$

The weight will always *oppose* any deformation of the masonry structure. For instance, with reference to Fig. 2.43, conditions (2.71') or (2.71'') imply that the pressure line, corresponding to the weight \mathbf{g} , will always be contained within the arch. In particular, condition (2.71'') dictates that the pressure curve can never touch the arch extrados or intrados, at any section, as shown in Fig. 2.44.

In the case of the arch illustrated in Fig. 2.44, the weight \mathbf{g} , evaluated per unit length on the horizontal projection, is symmetrical and increases from the key to the springers. All kinematically admissible mechanisms develop vertical displacements in which lifting is dominant. It is thereby clear why arch equilibrium is as a rule strictly admissible under their own weight alone, unless, of course, the arch is too slender. Live loads, \mathbf{q} , can exert a pushing action along mechanisms. Thus, for any assigned distribution of live loads \mathbf{q} , it is admissible that at least one mechanism exist along which load \mathbf{q} will do positive work.

The contribution to resistance of the weight \mathbf{g} come by virtue of the structure's *geometry*. Masonry structures must be designed so that the mechanisms produce vertical displacements in which lifting is always dominant, thereby satisfying condition (2.87) for any mechanism. It is the *geometry* alone that ensures that the structure's weight counters the emergence of any mechanisms.

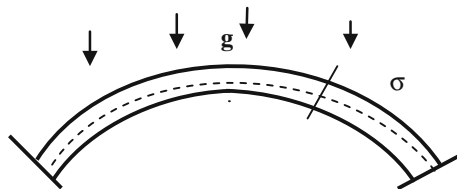


Fig. 2.44 Pressure line strictly contained within the arch

2.5.8 Mechanism States

The previous Fig. 2.41 shows the sketch of a masonry arch in equilibrium under loads \mathbf{p} and having its pressure line wholly contained within its thickness. In this state internal stresses oppose any deformation of the arch. It is however possible that a structure in admissible equilibrium under loads \mathbf{p} be freely deformed by a given mechanism displacement \mathbf{u}_m , defined by an arbitrary constant. In such a state, instead, the internal stresses and constraint reactions do not counter the emergence of the mechanism. Such a masonry structure is said to be in a *mechanism state* defined by the displacement \mathbf{u}_m . The mechanism, which implies the occurrence of a small movement of the structure while the admissible equilibrium is maintained, has arbitrary magnitude.

More precisely, the mechanism state, defined by the displacement field \mathbf{u}_m , is considered to be effectively activated in any body in admissible equilibrium under the loads \mathbf{p} when the following conditions are simultaneously satisfied:

- equilibrium between loads \mathbf{p} and internal stresses $\boldsymbol{\sigma}$

$$\langle \boldsymbol{\sigma}, \delta \boldsymbol{\varepsilon} \rangle = \{ \mathbf{t}^{(n^+)}, \Delta^{(n^-)} \delta \mathbf{u} \} + \langle \mathbf{r}, \delta \mathbf{u} \rangle + \langle \mathbf{p}, \delta \mathbf{u} \rangle \quad \forall \delta \mathbf{u} \in M; \quad (2.89)$$

- admissibility of the internal stress state

$$\langle \boldsymbol{\sigma}, \delta \boldsymbol{\varepsilon} \rangle \leq 0 \quad \{ \mathbf{t}^{(n^+)}, \Delta^{(n^-)} \delta \mathbf{u} \} \geq 0 \quad \langle \mathbf{r}, \delta \mathbf{u} \rangle \geq 0; \quad (2.90)$$

- lack of opposition by the internal stresses to activation of the mechanism displacement \mathbf{u}_m

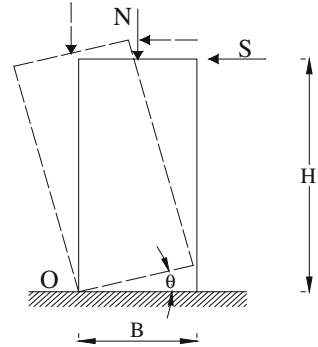
$$\begin{aligned} \{ \mathbf{t}^{(n^+)}(P^+), \Delta^{(n^-)} \mathbf{u}_m(P^-) \} &= 0, & P^+, P^- \in \Gamma(\mathbf{u}_m) \\ \langle \boldsymbol{\sigma}(P), \boldsymbol{\varepsilon}(\mathbf{u}_m(P)) \rangle &= 0, & P \in \Omega(\mathbf{u}_m); \\ \langle \mathbf{r}(P), \mathbf{u}_m(P) \rangle &= 0, & P \in \partial\Omega_r. \end{aligned} \quad (2.91)$$

Conditions (2.89), (2.90) and (2.91) are not altered if the mechanism displacement \mathbf{u}_m is affected by a constant factor: the displacement \mathbf{u}_m , which is small with respect to the structure's dimensions, thus has indefinite amplitude.

One consequence of conditions (2.91) is that the external loads \mathbf{p} also offer no opposition to the development of the mechanism displacement \mathbf{u}_m . In fact, setting $\delta \mathbf{u} = \mathbf{u}_m$, conditions (2.89) and (2.91) yield

$$\langle \mathbf{p}, \mathbf{u}_m \rangle = 0 \quad (2.92)$$

Fig. 2.45 Pier failure under force S



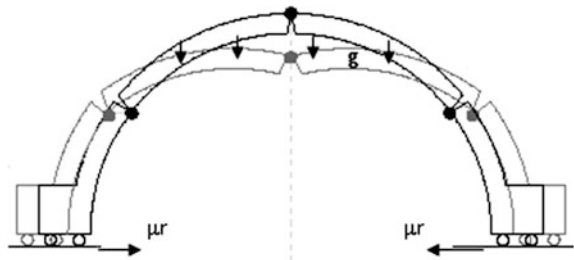
A mechanism state occurs in masonry structures under various peculiar equilibrium conditions, for example, just at the limit equilibrium attained upon collapse, or due to settling, as shown schematically in the two sketches in Figs. 2.43 and 2.44. Figure 2.45 shows the state of a masonry pier loaded by a central vertical force N and a horizontal one,

$$S = NB/2H. \tag{2.93}$$

The value of S has been chosen so that the resultant of N and S passes precisely through the toe O . The internal forces are due to axial force N and shear S : at the base section their resultant passes through the toe O . The mechanism v_c is represented by the counterclockwise rotation of the pier around the hinge at O . No detachment strain occurs at any section of the panel except at its base: here the resultant of the stresses passes exactly through O . The mechanism condition (2.92) is thus satisfied. The pier is at a mechanism state under loads N and S and can rotate in the counterclockwise direction around hinge O .

The case shown in Fig. 2.46 shows another example of a mechanism state differing from the previous condition of limit equilibrium. A slight increase in the span of an arch has been caused by settling of its foundation.

Fig. 2.46 The settled arch



The arch, now free at its springings, is loaded by the forces \mathbf{g} and the thrust $\mu\mathbf{r}$. The pressure line of the arch, without ever leaving the interior of the arch thickness, passes through the hinges indicated in the figure. The arch is thus in a mechanism state. The extension of the span of the arch can increase arbitrarily under the action of the constant loads \mathbf{q} and the constant thrust $\mu\mathbf{r}$.

2.6 Collapse State

2.6.1 Definitions

Let us now consider a masonry structure under a loading path $\mathbf{p}(\lambda)$, with λ the loading parameter. According to (2.86), we assume that the loads $\mathbf{p}(\lambda)$ are made up of the resistant component \mathbf{g} , i.e. the dead loads, and the pushing forces $\lambda\mathbf{q}$. We moreover assume that by increasing λ , the structure, initially in a *safe* AE state, will pass through a sequence of safe admissible equilibrium states, in the sense that condition (2.71) will always be satisfied in the strict form:

$$\langle \mathbf{g} + \lambda\mathbf{q}, \delta\mathbf{u} \rangle < 0, \quad \lambda > 0, \quad \forall \delta\mathbf{u} \in M. \quad (2.94)$$

Lastly, we assume that at some point during the loading process, when λ attains a critical value λ_c , the structure will *reach a mechanism state* defined by the mechanism \mathbf{u}_c . It is moreover admissible for the live loads, \mathbf{q} , to *push* along \mathbf{u}_c , or in other terms that

$$\langle \mathbf{q}, \mathbf{u}_c \rangle > 0. \quad (2.95)$$

Consequently, at $\lambda = \lambda_c$, condition (2.94) continues to be satisfied along all mechanisms other than \mathbf{u}_c , so that

$$\langle \mathbf{g} + \lambda_c\mathbf{q}, \delta\mathbf{u} \rangle < 0, \quad \lambda_c > 0, \quad \forall \delta\mathbf{u} \neq \mathbf{u}_c \in M, \quad (2.96)$$

while, on the contrary, the work done by the forces $\mathbf{p} = \mathbf{g} + \lambda_c\mathbf{q}$ vanishes along the mechanism \mathbf{u}_c , which is to say

$$\langle \mathbf{g} + \lambda_c\mathbf{q}, \mathbf{u}_c \rangle = 0, \quad \lambda_c > 0, \quad \mathbf{u}_c \in M. \quad (2.97)$$

Thus, as soon as the loading parameter λ is further increased beyond λ_c , by accounting for (2.95), we have

$$\left(\frac{d}{d\lambda} \langle \mathbf{p}(\lambda), \mathbf{u}_c \rangle \right)_{\lambda_c} = \langle \mathbf{q}, \mathbf{u}_c \rangle > 0. \quad (2.98)$$

Accordingly, condition (2.71), necessary and sufficient for the *existence of an admissible equilibrium state*, is violated and the structure *collapses*. At this collapse state an exchange occurs from conditions of existence to those of non-existence of

an admissible equilibrium state. Condition (2.95) evidences the presence of a pushing action by live loads, \mathbf{q} along displacement \mathbf{u}_c , the *failure mechanism*.

The *development* of this displacement can be represented by a sequence $k\mathbf{u}_c$ of mechanisms of increasing amplitude. Collapse thus occurs under *constant loads*, because by gradually increasing the constant $k > 0$, we consistently have

$$\langle \mathbf{g}, k\mathbf{u}_c \rangle + \lambda_c \langle \mathbf{q}, k\mathbf{u}_c \rangle = 0, \quad k\mathbf{u}_c \in M, k > 0 \quad (2.97')$$

for any amplitude of mechanism $k\mathbf{u}_c$. Constant loads also imply constant stresses. The failure mechanism thus develops under frozen loads and stresses. There is no energy dissipation at collapse. Nevertheless, the masonry structure is able to maintain its limit strength during the development of the failure mechanism, as occurs for a steel bar upon yielding.

Despite the lack of dissipation, the behavior at collapse of masonry structures is similar to that of ductile steel structures, as predicted by Limit Analysis.

The possibility of reaching collapse during a loading process represents the *most relevant aspect* of the behavior of masonry structures: for such structures, weight and geometry are the only strength resources countering failure.

Summing up all the foregoing general assumptions, it can be stated that a collapse state under loads $\mathbf{g} + \lambda_c \mathbf{q}$, is attained when the following four conditions are satisfied simultaneously:

- (1) *equilibrium under loads $\mathbf{g} + \lambda_c \mathbf{q}$ and stresses σ_c .*
Consequently, the virtual work equation holds

$$\langle \sigma_c(P), \varepsilon(\delta \mathbf{u}) \rangle = \langle \mathbf{g}, \delta \mathbf{u} \rangle + \lambda_c \langle \mathbf{q}, \delta \mathbf{u} \rangle, \quad \forall \delta \mathbf{u} \in M; \quad (2.99)$$

- (2) *compatibility of internal stresses σ_c*

$$\langle \sigma_c(P), \varepsilon(\delta \mathbf{u}) \rangle \leq 0; \quad (2.100)$$

- (3) *existence of a mechanism state \mathbf{u}_c under loadings $\mathbf{g} + \lambda_c \mathbf{q}$:*

$$\exists \mathbf{u}_c \in M : \langle \sigma_c, \varepsilon(\mathbf{u}_c) \rangle = 0; \quad (2.101)$$

- (4) *positive work performed by live loads \mathbf{q} along mechanism \mathbf{u}_c :*

$$\langle \mathbf{q}, \mathbf{u}_c \rangle > 0. \quad (2.102)$$

In the following, we will prove the *static* and the *kinematic* theorems of Limit Analysis in their specific form for masonry structures. The earliest proofs of the validity of Limit Analysis to masonry structures dates back to Kooharian (1954), Prager (1959) and Heyman (1966).

The proofs described in the next sections follow the lines of reasoning formulated by Como (1992, 1996a, b). A number of different checks of the theorems have been provided within the no-tension framework by others, such as for example, Sinopoli et al. (1998).

2.6.2 The Static Theorem

Let us consider a masonry structure loaded by fixed dead loads \mathbf{g} and the additional live load $\lambda^- \mathbf{q}$, with λ^- the multiplier of loads \mathbf{q} . A given known stress distribution $\boldsymbol{\sigma}^-$ is in an admissible equilibrium with the assigned loads. The statement of the theorem is thus the following:

The loads $\mathbf{g} + \lambda^- \mathbf{q}$ are not greater than the collapse loads if admissible equilibrium exists between the loads $\mathbf{g} + \lambda^- \mathbf{q}$ and the internal stresses $\boldsymbol{\sigma}^-(P)$

The assumptions underlying the theorem are:

- equilibrium between $\mathbf{g} + \lambda^- \mathbf{q}$ and $\boldsymbol{\sigma}^-(P)$:

$$\langle \boldsymbol{\sigma}^-(P), \boldsymbol{\varepsilon}(\delta \mathbf{u}) \rangle = \langle \mathbf{g}, \delta \mathbf{u} \rangle + \lambda^- \langle \mathbf{q}, \delta \mathbf{u} \rangle \quad \forall \delta \mathbf{u} \in M \quad (2.103)$$

- static compatibility of stresses $\boldsymbol{\sigma}^-(P)$:

$$\langle \boldsymbol{\sigma}^-(P), \boldsymbol{\varepsilon}(\delta \mathbf{u}) \rangle \leq 0, \quad \forall \delta \mathbf{u} \in M. \quad (2.104)$$

Together, assumptions (2.103) and (2.104) yield:

$$\lambda^- \leq \lambda_c. \quad (2.105)$$

The proof of the theorem starts by considering that at collapse, under loads

$$\mathbf{g} + \lambda_c \mathbf{q},$$

the following condition will be satisfied

$$\langle \boldsymbol{\sigma}_c(P), \boldsymbol{\varepsilon}(\mathbf{u}_c) \rangle = \langle \mathbf{g}, \mathbf{u}_c \rangle + \lambda_c \langle \mathbf{q}, \mathbf{u}_c \rangle. \quad (2.106)$$

Such condition, in which $\boldsymbol{\sigma}_c$ denotes the corresponding stresses, is obtained by applying the virtual work equation to the collapse state with $\delta \mathbf{u} = \mathbf{u}_c$.

At collapse, however, the mechanism condition (2.101) also holds, because the internal stresses $\boldsymbol{\sigma}_c$ do not oppose the development of the mechanism \mathbf{u}_c . Consequently, from (2.106) we get

$$0 = \langle \mathbf{g}, \mathbf{u}_c \rangle + \lambda_c \langle \mathbf{q}, \mathbf{u}_c \rangle. \quad (2.99')$$

Furthermore, taking into account the assumed existence of admissible equilibrium between the loads $\mathbf{g} + \lambda^- \mathbf{q}$ and the internal stresses $\boldsymbol{\sigma}^-$, from (2.103) with $\delta \mathbf{u} = \mathbf{u}_c$, we obtain

$$\langle \boldsymbol{\sigma}^-(P), \boldsymbol{\varepsilon}(\mathbf{u}_c) \rangle = \langle \mathbf{g}, \mathbf{u}_c \rangle + \lambda^- \langle \mathbf{q}, \mathbf{u}_c \rangle. \quad (2.107)$$

By subtracting the previous equality (2.99') from this, we get

$$\langle \boldsymbol{\sigma}^-(P), \boldsymbol{\varepsilon}(\mathbf{u}_c) \rangle = (\lambda^- - \lambda_c) \langle \mathbf{q}, \mathbf{u}_c \rangle. \quad (2.108)$$

On the other hand, the static compatibility of stresses $\boldsymbol{\sigma}^-(P)$, expressed by inequality (2.104) with $\delta \mathbf{u} = \mathbf{u}_c$, gives

$$\langle \boldsymbol{\sigma}^-(P), \boldsymbol{\varepsilon}(\mathbf{u}_c) \rangle \leq 0 \quad (2.109)$$

whence, from (2.108)

$$(\lambda^- - \lambda_c) \langle \mathbf{q}, \mathbf{u}_c \rangle \leq 0. \quad (2.110)$$

At collapse, according to (2.102), the work of the live loads \mathbf{q} along the failure mechanism \mathbf{u}_c is positive; thus, from (2.110) we have $(\lambda^- - \lambda_c) \leq 0$, or

$$\lambda^- \leq \lambda_c. \quad (2.111)$$

The static multiplier λ^- is thus *not greater* than the collapse multiplier λ_c . The static theorem is one of most important theorems in Structural Engineering. Frequently, when checking the behavior of complex structures under the action of given load distributions, we make conjectures about different internal resistant systems, many of which are unable to sustain the loads (with the exception of at least one).

The static theorem, perhaps surprisingly, tells us that the structure will not fail; that it is certainly able to produce at least one resistant system able to support the loads (though not necessarily the one identified).

The search for states of admissible equilibrium by applying the static theorem begins with construction of a preliminary equilibrium configuration of the structure, for instance, by using funicular polygons, and then verifying its static admissibility. For example, in the case of an arch under given loads, a funicular curve of the load distribution is first drawn and then checked to see whether it is wholly contained within the arch. If it is, the loads are not greater than the collapse ones and the structure is in equilibrium.

2.6.3 The Kinematic Theorem

Assuming that a structure is in a *mechanism state* under loads $\mathbf{g} + \lambda^+ \mathbf{q}$ along a given mechanism \mathbf{u}^+ , the multiplier λ^+ is initially unknown. However, according to (2.92), we have

$$0 = \langle \mathbf{g}, \mathbf{u}^+ \rangle + \lambda^+ \langle \mathbf{q}, \mathbf{u}^+ \rangle \quad (2.112)$$

and the kinematic multiplier λ^+ , satisfying (2.112), is thus defined as

$$\lambda^+ = - \frac{\langle \mathbf{g}, \mathbf{u}^+ \rangle}{\langle \mathbf{q}, \mathbf{u}^+ \rangle} \quad (2.113)$$

Condition (2.112) implies equilibrium along the mechanism \mathbf{u}^+ between the pushing load $\lambda^+ \mathbf{q}$ and the resistant weights \mathbf{g} . We also assume that the loads \mathbf{q} push along \mathbf{u}^+ , hence

$$\langle \mathbf{q}, \mathbf{u}^+ \rangle > 0. \quad (2.114)$$

Under such conditions, the theorem states that the kinematic multiplier λ^+ cannot be lower than the collapse multiplier λ_c , that is,

$$\lambda^+ \geq \lambda_c. \quad (2.115)$$

Once again in this case the proof depends on conditions defining the collapse state, particularly the condition of limit equilibrium. Thus, from condition (2.99) with $\delta \mathbf{u} = \mathbf{u}^+$, we obtain

$$\langle \boldsymbol{\sigma}_c(P), \boldsymbol{\varepsilon}(\mathbf{u}^+) \rangle = \langle \mathbf{g}, \mathbf{u}^+ \rangle + \lambda_c \langle \mathbf{q}, \mathbf{u}^+ \rangle, \quad (2.99')$$

which by subtracting equality (2.112) yields

$$\langle \boldsymbol{\sigma}_c(P), \boldsymbol{\varepsilon}(\mathbf{u}^+) \rangle = (\lambda_c - \lambda^+) \langle \mathbf{q}, \mathbf{u}^+ \rangle. \quad (2.116)$$

On the other hand, simply because an admissible equilibrium still exists at collapse, from (2.100), with $\delta \mathbf{u} = \mathbf{u}^+$, we have

$$\langle \boldsymbol{\sigma}_c(P), \boldsymbol{\varepsilon}(\mathbf{u}^+) \rangle \leq 0, \quad (2.100')$$

and from (2.116) we obtain

$$(\lambda_c - \lambda^+) \langle \mathbf{q}, \mathbf{u}^+ \rangle \leq 0. \quad (2.116')$$

Hence, taking into account to our initial assumptions (2.114)

$$\lambda^+ \geq \lambda_c. \quad (2.117)$$

Multiplier λ^+ , i.e., the kinematically admissible multiplier of loads \mathbf{q} , represents the *upper bound* of the collapse multiplier λ_c .

2.6.4 Uniqueness of the Collapse Multiplier

Let us assume, *ad absurdum*, that two different values λ_{c1} and λ_{c2} of the collapse load multiplier exist. Both λ_{c1} and λ_{c2} satisfy the equilibrium conditions (2.99) between loads and stresses. Moreover, the stress compatibility conditions (2.100) are satisfied, as are conditions (2.101) required for the existence of the mechanism state, as well as (2.102). Let us now assume, for instance, that

$$\lambda_{c1} \leq \lambda_{c2}. \quad (2.118)$$

However, the failure multiplier λ_{c2} is also a statically admissible multiplier, since it satisfies the equilibrium conditions with the corresponding internal compatible stresses σ_{c1} . Thus, if λ_{c1} is a collapse multiplier, from (2.111) we also have

$$\lambda_{c2} \leq \lambda_{c1}. \quad (2.119)$$

Comparison of (2.118) with (2.119) yields

$$\lambda_{c1} = \lambda_{c2}.$$

The result should be the same if, on the contrary, it were assumed that $\lambda_{c2} \leq \lambda_{c1}$. The collapse multiplier is thus unique, though, in general, the failure mechanism is not.

The two theorems, static and kinematic, set a bounding interval for the collapse multiplier, because

$$\lambda^- \leq \lambda_c \leq \lambda^+. \quad (2.120)$$

It should be recognized that the collapse load does not depend on the material properties, but only on the geometry of the structure and the magnitude of the dead loads. Subsequent chapters will provide in-depth examples of the numerous applications of the theorems presented here.

2.6.5 Indeformable Systems: Lack of Collapse

Under the action of external loads, an *indeformable* system tends to become deformed, resulting in dilatation and cracking. On the other hand the interpenetration strength of the material, together with the presence of fixed constraints, prevents any deformation. Thus, only compressions can take place within the body. The indeformable structure will be thus always able to sustain the applied loads. Collapse mechanisms cannot therefore exist and such systems never fail, unless the material undergoes crushing or the constraints are displaced through settling.

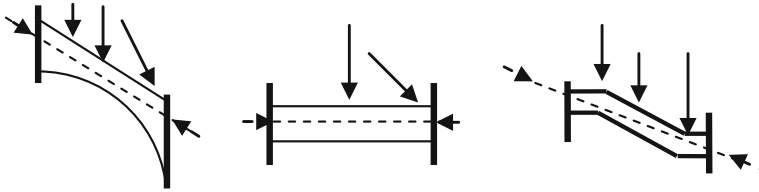


Fig. 2.47 Lack of collapse for indeformable systems

The same conclusion can be reached from another perspective. As noted previously, self-equilibrated stresses do exist in these systems. An arbitrary self-equilibrated stress distribution can be added to any stress field in equilibrium with the loads in such a way that the overall stress state turns out to be solely compressive. Referring to any of the three illustrations in Fig. 2.47, once a funicular polygon of the applied loads is traced, for instance, passing through the intrados at the springers and the extrados at the key section, we can apply two equal and opposite forces able to modify the polygon so that it remains entirely contained within the structure. These self-equilibrated stresses are produced by the same external loads that tend to deform the structure and force the external constraints. Such structures are thus able to sustain any load.

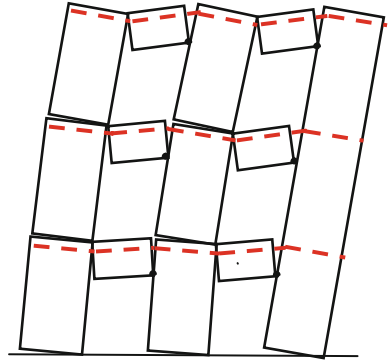
The real problem, on the other hand, is evaluating the most probable thrust transmitted by the structure at its supports. The indeterminacy of the static solutions can be overcome by seeking solutions within the framework of the principles of minimum thrust. The thrust also slightly deforms the supports and activates *minimum thrust states*.

It should lastly be noted that for such systems the usual assumption of infinitely strong masonry can be opportunely removed with in order to obtain more realistic evaluations of a structure's maximum capacity, as we will show in the next chapter.

2.6.6 Collapse State for the Elastic No Tension Systems

The definition of collapse state given at Sect. 2.6.1 for the rigid in compression no tension bodies holds also for the elastic no tension systems. During the loading failure is met when a mechanism \mathbf{u}_c turns up along which the structure deforms under constant loads $\mathbf{g} + \lambda_c \mathbf{q}$ and, consequently, under constant stresses. *No elastic strain increments $\Delta\sigma$ take place at the collapse*. To prove this statement, let us admit, by contradiction, that the failure displacement is composed both by cracking and elastic strain increments $\boldsymbol{\varepsilon}_f(\mathbf{u}_c)$ and $\boldsymbol{\varepsilon}_e(\mathbf{u}_c)$. Thus, if the stress increment $\Delta\boldsymbol{\sigma}$ takes place, the equilibrium condition under constant loads and along the failure displacement \mathbf{u}_c gives

Fig. 2.48 Failure of a masonry wall reinforced by steel ties. During the mechanism, plastic stretching occurs in the steel ties



$$\langle \Delta \boldsymbol{\sigma}, \boldsymbol{\varepsilon}_f(\mathbf{u}_c) \rangle + \langle \Delta \boldsymbol{\sigma}, \boldsymbol{\varepsilon}_e(\mathbf{u}_c) \rangle = 0 \quad (2.121)$$

But along the failure displacement we have

$$\langle \Delta \boldsymbol{\sigma}, \boldsymbol{\varepsilon}_f(\mathbf{u}_c) \rangle = 0 \quad (2.122)$$

because the stress increments $\Delta \boldsymbol{\sigma}$ cannot oppose the opening deformations of the structure. Hence, condition (2.123) becomes

$$\langle \Delta \boldsymbol{\sigma}, \boldsymbol{\varepsilon}_e(\mathbf{u}_c) \rangle = 0 \quad (2.123)$$

But this result cannot occur because, when elastic strains take place, the work $\langle \Delta \boldsymbol{\sigma}, \boldsymbol{\varepsilon}_e(\mathbf{u}_c) \rangle$ represents a positive elastic strain energy. Thus

$$\Delta \boldsymbol{\sigma} = 0 \quad (2.124)$$

The failure of the elastic no tension systems thus occurs with a mechanism displacement, in absence of elastic strain. Internal stresses maintain frozen during the collapse. This result is useful for a better understanding of the behaviour at the collapse of masonry structures reinforced by elasto-plastic systems, as for instance, steel ties (Fig. 2.48). At the collapse these devices, at the plastic state, follow at constant stress the occurrence of the failure mechanism.

2.7 Incipient Settled States

2.7.1 Definitions

Let us consider a masonry structure at a *safe admissible equilibrium* state at configuration C_i under the actions of loads \mathbf{g} and the corresponding internal stresses $\boldsymbol{\sigma}_i$. For deformable systems inequality (2.71') holds, so we have

$$\langle \mathbf{g}, \delta \mathbf{u} \rangle < 0, \quad \forall \delta \mathbf{u} \in M. \tag{2.125}$$

Evidently, according to Sect. 2.6.5, the assumption of a safe admissible equilibrium state at the initial configuration C_i under the loads \mathbf{g} is still valid also if the structure, for its initial constraint conditions, is indeformable. Recall that the equilibrium at C_i is *safe* because no mechanism exists along which the work of loads \mathbf{g} vanishes.

Let us now assume that the structure becomes slightly deformed as a consequence of the incipient *settlement mechanism*, \mathbf{v}_s , occurring at one of its external constraints. By way of example, consider the arch in Fig. 2.49, which undergoes a slight increase in span due to settling.

Let C_s be the configuration taken on by the structure once settlement has occurred. By assuming that C_s is *very near* C_i , we can refer to the geometry of the initial configuration C_i when expressing the equilibrium equations. The settlement mechanism, \mathbf{v}_s , is the displacement field that moves the structure from C_i to C_s .

As the settlement occurs, the structure's internal equilibrium shifts from initial configuration C_i to the displaced one C_s . Changes in the internal stresses and constraint reactions will occur during the transition from C_i to C_s , so that the initial stress state, σ_i , admissible and in equilibrium with loads \mathbf{g} , is altered and becomes

$$\sigma_s.$$

This internal stress state, σ_s , which accounts for settlement \mathbf{v}_s , is statically admissible and thus satisfies the inequality

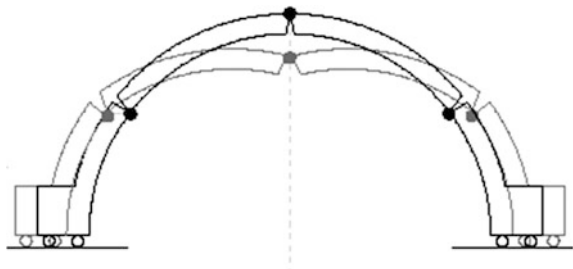
$$\langle \sigma_s, \varepsilon(\delta \mathbf{u}) \rangle \leq 0 \tag{2.126}$$

Likewise, the settled constraint, which *before* the settling, produced the reaction $\mu_i \mathbf{r}$, *after* the settling produces the new reaction

$$\mu_s \mathbf{r}, \tag{2.127}$$

where \mathbf{r} is a given force having the direction of reaction of the settled constraint and μ is the corresponding multiplier. In brief, during the development of the settlement mechanism, \mathbf{v}_s , the structure will remain in a state of admissible equilibrium while

Fig. 2.49 Arch with increased span due to settling at its springers



the stresses vary from $\boldsymbol{\sigma}_i$ to $\boldsymbol{\sigma}_s$, the corresponding pressure line shifts from π_i to π_s , and the reaction of the settled constraint changes from $\mu_i \mathbf{r}$ to $\mu_s \mathbf{r}$.

In the case of the masonry arch that has undergone a slight increase in span, its pressure line π_s will pass through the hinges corresponding to mechanism \mathbf{v}_s . Consequently, no work will be done by the internal stresses $\boldsymbol{\sigma}_s$ on the deformations corresponding to \mathbf{v}_s . The same occurs for any structure that is slightly deformed by a mechanism and adapts itself to settling. Thus, at the settlement state the following *mechanism state* holds

$$\langle \boldsymbol{\sigma}_s, \boldsymbol{\varepsilon}(\mathbf{v}_s) \rangle = 0. \quad (2.128)$$

We can *release* the structure by removing the settled configuration constraint by applying the reaction $\mu_s \mathbf{r}$ to the eliminated constraint. The set of all mechanisms of the released structure is denoted by \bar{M} . In the released structure in the settled state, the applied loads are represented by both the weights \mathbf{g} and the reactions $\mu_s \mathbf{r}$. Thus, considering the released structure in the admissible settled equilibrium state, from the virtual work equation we get

$$\langle \mathbf{g}, \delta \mathbf{u} \rangle + \mu_s \langle \mathbf{r}, \delta \mathbf{u} \rangle = \langle \boldsymbol{\sigma}_s, \boldsymbol{\varepsilon}(\delta \mathbf{u}) \rangle, \quad \forall \delta \mathbf{u} \in \bar{M}, \quad (2.129)$$

which for $\delta \mathbf{u} = \mathbf{v}_s$, according to (2.128), yields

$$\langle \mathbf{g}, \mathbf{v}_s \rangle + \mu_s \langle \mathbf{r}, \mathbf{v}_s \rangle = 0. \quad (2.130)$$

Loads \mathbf{g} perform positive work along the mechanism displacements \mathbf{v}_s , while the reaction $\mu_s \mathbf{r}$ of the released constraint opposes settling, so that

$$\langle \mathbf{g}, \mathbf{v}_s \rangle > 0 \quad (2.131)$$

and

$$\mu_s \langle \mathbf{r}, \mathbf{v}_s \rangle < 0. \quad (2.132)$$

An *admissible settlement equilibrium state* is therefore defined once the mechanism settlement \mathbf{v}_s has taken place. Conditions (2.126–2.132), define the *admissible settlement equilibrium state*.

2.7.2 Features of Incipient Settled States

Firstly, once the slight settlement, \mathbf{v}_s , has occurred and the structure has shifted into configuration C_s , the settled constraint can once again be made active.

In spite of the settling that occurred, the work of the loads due to any mechanism, $\delta \mathbf{u}$ is still the same as the work evaluated at the initial configuration C_i , assuming, of course, that displacements, \mathbf{v}_s , are *very small* (as stated above) and that

the changes in geometry are consequently *negligible*. Thus, if at the initial state C_i , the admissibility condition $\langle \mathbf{g}, \delta \mathbf{u} \rangle < 0, \forall \delta \mathbf{u} \in M$ is satisfied, the same condition will still be satisfied by the new configuration C_s . In this regard, recall Heyman's statement (1966): "*if the foundations of a stone structure are liable to small movements, such movements will never, of themselves, promote the collapse of the structure*". Moreover, if settlement \mathbf{v}_s returns, increases and becomes

$$k\mathbf{v}_s, \quad k > 1, \quad (2.133)$$

the static arrangement of the structure will not change, and the internal stresses will remain fixed at σ_s . Indeed, as the stresses σ_s are forced to satisfy condition (2.128), they will continue to satisfy the same condition when the structure deforms by displacements k times larger than the prior ones. Thus, if the pressure curve skims the extrados and the intrados of the arch at the hinges corresponding to mechanism \mathbf{v}_s , and condition (2.128) is consequently satisfied, the same condition (2.128) will continue to be satisfied by assuming the mechanisms $k\mathbf{v}_s, k > 1$. Consequently the work of the same stresses, σ_s , on the deformations associated to displacements $k\mathbf{v}_s$ continues to be zero. Likewise, the thrust $\mu_s \mathbf{r}$, which according to (2.129), satisfies the equilibrium with the loads \mathbf{g} along the displacements \mathbf{v}_s , will continue to satisfy the same equilibrium condition (2.129) along the displacement field $k\mathbf{v}_s, k > 1$. In short, the structure freely follows any increase in the settlement, maintaining its configuration in admissible equilibrium: settling develops with frozen internal stresses, σ_s , and constraint reactions, $\mu_s \mathbf{r}$. The actual degree of settling is difficult to quantify. Despite this uncertainty, the internal stress state of the structure is, to the contrary, well-defined. No equilibrium loss will occur during the settling. This is a peculiar aspect of masonry structures that can explain the great durability and longevity of so many historic buildings. *How do we evaluate this stress state and the corresponding reaction of the settled restraint?* The answer to this question will be provided in the following sections.

2.7.3 *Statically Admissible Thrusts: The Static Theorem of Minimum Thrust*

Let us now look at the static equilibrium of a structure that has previously undergone settling. Two relevant examples are represented by a masonry arch whose span is lengthened by settling at the springings and the vertical settlement of the central pier of a masonry bridge. The settled structure is certainly at AE equilibrium under the loads \mathbf{g} and internal stresses σ . We know, a priori, nothing about the internal stresses σ occurring in the settled state, except that they are statically admissible. Let S be the set of all statically admissible internal stresses, σ , with $\sigma \in S$. We choose any one such distribution of statically admissible stresses σ . A thrust $\mu \mathbf{r}$ of the released constraint will correspond unequivocally to this distribution, hence let

$$\mu \mathbf{r}(\boldsymbol{\sigma} \in S) \quad (2.134)$$

be the reaction of the settled constraint associated to the statically admissible stresses $\boldsymbol{\sigma}$. For any $\boldsymbol{\sigma} \in S$, we can associate the reaction $\mu \mathbf{r}(\boldsymbol{\sigma} \in S)$, which defines the thrust of the settled constraint.

According to our assumptions, in the released structure the following equation between loads \mathbf{g} , internal stresses $\boldsymbol{\sigma}$ and the corresponding thrust $\mu \mathbf{r}(\boldsymbol{\sigma} \in S)$ for the AE holds

$$\langle \mathbf{g}, \delta \mathbf{u} \rangle + \mu \mathbf{r}(\boldsymbol{\sigma}) \langle \mathbf{r}, \delta \mathbf{u} \rangle = \langle \boldsymbol{\sigma}, \boldsymbol{\varepsilon}(\delta \mathbf{u}) \rangle, \quad \boldsymbol{\sigma} \in S, \quad \forall \delta \mathbf{u} \in \bar{M}. \quad (2.135)$$

Moreover, the following inequality

$$\langle \boldsymbol{\sigma}, \boldsymbol{\varepsilon}(\delta \mathbf{u}) \rangle \leq 0 \quad \forall \delta \mathbf{u} \in \bar{M} \quad (2.136)$$

will also be satisfied for the admissibility of the stresses $\boldsymbol{\sigma} \in S$. Thrust $\mu \mathbf{r}(\boldsymbol{\sigma} \in S)$, in equilibrium with loads \mathbf{g} and internal stresses $\boldsymbol{\sigma}$, that is to say, satisfying condition (2.135), represents *any state of statically admissible thrust*. Now, of all the statically admissible thrusts, which one corresponds to the settled state?

We know that the actual thrust in the settled state corresponds to an admissible stress state that *does no work* on the deformations occurring during the settlement mechanism, that is, it satisfies (2.128). If we define \mathbf{v}_s as the effective settlement mechanism, we specify condition (2.135) using $\delta \mathbf{u} = \mathbf{v}_s$ to obtain

$$\langle \mathbf{g}, \mathbf{v}_s \rangle + \mu(\boldsymbol{\sigma}) \langle \mathbf{r}, \mathbf{v}_s \rangle = \langle \boldsymbol{\sigma}, \boldsymbol{\varepsilon}(\mathbf{v}_s) \rangle \quad \boldsymbol{\sigma} \in S. \quad (2.137)$$

We now subtract equality (2.130), regarding the actual settlement state, from equality (2.137) to obtain

$$(\mu(\boldsymbol{\sigma}) - \mu_s) \langle \mathbf{r}, \mathbf{v}_s \rangle = \langle \boldsymbol{\sigma}, \boldsymbol{\varepsilon}(\mathbf{v}_s) \rangle \quad \boldsymbol{\sigma} \in S. \quad (2.138)$$

By taking (2.136) into account, from (2.138), with $\delta \mathbf{u} = \mathbf{v}_s$, we get

$$(\mu(\boldsymbol{\sigma}) - \mu_s) \langle \mathbf{r}, \mathbf{v}_s \rangle \leq 0 \quad \boldsymbol{\sigma} \in S, \quad (2.139)$$

and by virtue of (2.132), we obtain

$$\mu_s \leq \mu(\boldsymbol{\sigma}) \quad \boldsymbol{\sigma} \in S \quad (2.140)$$

The multiplier, μ_s , of the settled thrust \mathbf{r} is thus *lower* than all the statically admissible multipliers μ . The thrust in the settled state is consequently the lowest of all the statically admissible thrusts.

This finding (Como 1996a, b, 1998) relates to a previously described, well-known property of masonry arches that undergo an increase in span due to

settling at the springings: such an arch is in the state of minimum thrust because its pressure line corresponds to the minimum span and the maximum sag, as shown by Heyman (1966).

2.7.4 *Kinematically Admissible Thrusts: The Kinematic Theorem of the Minimum Thrust*

Let us now examine the settlement equilibrium state from a *kinematic* point of view. The actual settlement mechanism is unknown: for instance, for the case of the arch, we cannot know the position of the internal hinge. We only know that, during the development of the mechanism, loads \mathbf{g} will do positive work, while the work of the reaction of the settled constraint is, to the contrary, negative.

Let \bar{M} be the set of all kinematically admissible settlement mechanisms of the released structure: they do not allow for any internal interpenetration of masonry and respect all the restrictions for the other unsettled constraints. Let us consider some settlement mechanism

$$\mathbf{v} \in \bar{M} \quad (2.141)$$

of the released structure. The loads \mathbf{g} will push along \mathbf{v} and consequently

$$\langle \mathbf{g}, \mathbf{v} \rangle > 0. \quad (2.142)$$

We define the *kinematic multiplier*, λ , of the reaction \mathbf{r} of the settled constraint as that multiplier able to ensure equilibrium of the structure along the assumed settlement mechanism, \mathbf{v} , or, in other terms, that the following condition holds

$$\langle \mathbf{g}, \mathbf{v} \rangle + \lambda \langle \mathbf{r}, \mathbf{v} \rangle = 0. \quad (2.143)$$

Reaction $\lambda \mathbf{r}(\mathbf{v})$ opposes the development of settling, \mathbf{v} , given that, by taking (2.142) into account, we get

$$\lambda \langle \mathbf{r}, \mathbf{v} \rangle < 0. \quad (2.144)$$

where \mathbf{r} is any resistant reaction of the settled constraint. The kinematic multiplier $\lambda(\mathbf{v})$ of reaction \mathbf{r} is thus defined as

$$\lambda(\mathbf{v}) = -\frac{\langle \mathbf{g}, \mathbf{v} \rangle}{\langle \mathbf{r}, \mathbf{v} \rangle}, \quad \mathbf{v} \in \bar{M}. \quad (2.145)$$

Let us now search for the conditions under which kinematic reaction $\lambda \mathbf{r}(\mathbf{v})$ may represent the actual settled state. This latter is represented by the reaction, $\mu_s \mathbf{r}$, that

satisfies the foregoing settlement conditions (2.126), (2.128), (2.129), (2.130), (2.131) and (2.132). Thus, let us assume $\delta \mathbf{u} = \mathbf{v}$ in (2.139) to get

$$\langle \mathbf{g}, \mathbf{v} \rangle + \mu_s \langle \mathbf{r}, \mathbf{v} \rangle = \langle \boldsymbol{\sigma}_s, \boldsymbol{\varepsilon}(\mathbf{v}) \rangle, \quad \mathbf{v} \in \bar{M}, \quad (2.146)$$

where, according to (2.126)

$$\langle \boldsymbol{\sigma}_s, \boldsymbol{\varepsilon}(\mathbf{v}) \rangle \leq 0 \quad \mathbf{v} \in \bar{M}. \quad (2.147)$$

Now, subtracting (2.143) from equality (2.146) yields

$$(\mu_s - \lambda(\mathbf{v})) \langle \mathbf{r}, \mathbf{v} \rangle = \langle \boldsymbol{\sigma}_s, \boldsymbol{\varepsilon}(\mathbf{v}) \rangle \quad \mathbf{v} \in \bar{M}. \quad (2.148)$$

Moreover, from (2.126), with $\delta \mathbf{u} = \mathbf{v}$, we get $(\mu_s - \lambda(\mathbf{v})) \langle \mathbf{r}, \mathbf{v} \rangle \leq 0$ and, consequently, from (2.144) (Como 1996a, b, 1998)

$$\mu_s \geq \lambda(\mathbf{v}) \quad \mathbf{v} \in \bar{M}. \quad (2.149)$$

For any settlement mechanism, $\mathbf{v} \in \bar{M}$, the corresponding kinematic multiplier, $\lambda(\mathbf{v} \in \bar{M})$, can never be greater than the actual settlement multiplier, μ_s . Thus μ_s is *the maximum* of all kinematic multipliers, $\lambda(\mathbf{v} \in \bar{M})$, for varying \mathbf{v} in the set of all settlement mechanisms \bar{M} , or in other terms

$$\mu_s = \text{MAX} \left(- \frac{\langle \mathbf{g}, \mathbf{v} \rangle}{\langle \mathbf{r}, \mathbf{v} \rangle} \right) \quad \mathbf{v} \in \bar{M}. \quad (2.150)$$

2.7.5 Uniqueness of the Settlement Multiplier

The proof of the uniqueness of the settlement multiplier follows the same path as that for the collapse multiplier.

2.7.6 The Class of the Statical and Kinematical Settlement Multipliers

$\lambda(\mathbf{v} \in \bar{M})$ is any admissible *kinematic* multiplier, defined according to (2.145). The corresponding thrust $\lambda(\mathbf{v} \in \bar{M}) \mathbf{r}$ is not, as a rule, statically admissible. Since

$$\lambda(\mathbf{v} \in \bar{M}) \leq \text{MAX} \lambda(\mathbf{v} \in \bar{M}) = \mu_s, \quad (2.151)$$

the thrust $\lambda(\mathbf{v} \in \bar{M}) \mathbf{r}$ is weaker than the minimum thrust $\mu_s \mathbf{r}$. Moreover, $\mu(\boldsymbol{\sigma} \in S)$ is any *statically* admissible multiplier that, according to previous definitions, is not

kinematically admissible, in the sense that the internal stresses are not generally associated to a mechanism. In the case of an arch, for instance, the pressure line corresponding to the stress distribution, $\sigma \in S$, does not skim the extrados and intrados of the arch to form hinges in numbers sufficient to produce a kinematically admissible mechanism. The thrust $\mu(\sigma)\mathbf{r}$ is greater than the minimum $\mu_s\mathbf{r}$ and

$$\mu_s = \underset{\sigma}{\text{MIN}} \mu(\sigma) \leq \mu(\sigma). \quad (2.152)$$

In conclusion, we obtain

$$\lambda(\mathbf{v}) \leq \text{MAX} \lambda(\mathbf{v}) = \mu_s = \text{MIN} \mu(\sigma) \leq \mu(\sigma). \quad (2.153)$$

The actual settlement mechanism, \mathbf{v}_s , together with the reaction of the settled constraint, may be determined via (2.153). These results will be applied in the following to analyze the statics of a number of masonry structures.

The problem of the evaluation of the minimum thrust for the rounded arch was analyzed by Coulomb (1773). Coulomb guessed that such a state was reached by the settled arch that endured a light widening at its springers. The pressure line touches the intrados and the extrados of the arch to form the hinges of the settlement mechanism. Figure 2.57 shows the rounded arch with the three hinges symmetrically placed. The position of the hinge C, having distance d from the horizontal straight line passing through the key hinge A, is defined by the angle β .

Figure 2.57 shows the force V, resultant of the weights of the segment AC of the arch.

Position of V is given by its distance L_A from the internal hinge C. Coulomb, examining the equilibrium of the segment AC of the arch and for a given position of the hinge C, i.e. for a given β , valued the thrust of the arch as

$$H = \frac{VL_A}{d} \quad (2.154)$$

Thus thrust H depends on the angle β . Coulomb noticed, as pointed out by Ochsendorf (2006), that the minimum thrust of the arch was attained by the maximum of thrust (2.154) by varying the angle β , as shown in Fig. 2.57. This remark can be explained taking into account that the thrust (2.154) is just the kinematical thrust corresponding to definition (2.150). According to the kinematical theorem the minimum thrust has to be searched as the maximum of the kinematical ones

$$H_{\text{Min}} = \underset{\beta}{\text{Max}} H = \underset{\beta}{\text{Max}} \frac{\langle g, v \rangle}{\Delta} \quad (2.155)$$

Expression (2.155) corresponds to (2.154). In fact the work of the weight $g(x)$ of the arch along the vertical displacements $v(x)$ produced by the settlement mechanism is

$$\langle g, v \rangle = \theta \int_{AC} g(x) \cdot x \cdot dx \tag{2.156}$$

The force V is on the other hand defined as

$$V = \int_{AC} g(x) \cdot dx \tag{2.157}$$

The distance L_A

$$V \cdot L_A = \int_{AC} g(x) \cdot x \cdot dx \tag{2.158}$$

gives the position of the force V. Consequently we get, with (2.158) or

$$H = \frac{\theta \int_{AC} g(x) \cdot x \cdot dx}{d \cdot \vartheta} \tag{2.159}$$

Finally, taking into account that $\Delta = d \theta$ (Fig. 2.50) we can write

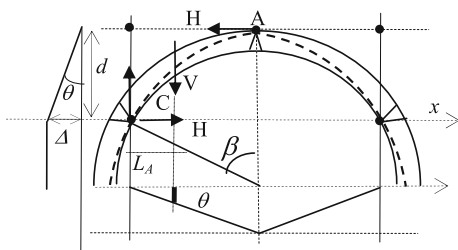
$$H = \frac{V \cdot L_A}{d} = \frac{\langle g, v \rangle}{\Delta} \tag{2.160}$$

The thrust (2.146) is properly the kinematical thrust defined by (2.140). On the other hand the minimumthrust of the arch is the maximum of all the kinematical thrusts H by varying the angle β , i.e. the position of the internal hinges C. Thus we have

$$H_{Min} = \underset{\beta}{Max} H = \underset{\beta}{Max} \frac{\langle g, v \rangle}{\Delta} \tag{2.161}$$

The kinematical thrust of the rounded arch of minimum thickness, i.e. with $t/R = 0.1075$, attains its maximum at the angle $\beta = 54.5^\circ$, (Ochsendorf 2006).

Fig. 2.50 The research of the minimum thrust of the arch



2.7.7 An Application of the Kinematic Approach. A Minimum Thrust Assessment

Let us consider the masonry bridge sketched out in Fig. 2.51. The bridge's central pier has undergone vertical settling. The settlement mechanism is traced out in the figure, where $\mu_s r$ indicates the vertical reaction of the central pier.

The figure also shows the critical sections where hinges are located: they are the two points O at the base corners of the right and left abutments, point A at the connection section between the abutments and girders, and point B at an intermediate section along the girder extrados. The distance between hinges B and C is denoted by x . The vertical settlement of the central pier defines the position of hinges O and A of the abutments, which will rotate outwardly. Hinges B, whose positions are instead unknown, are each at a distance $a + x$ from the internal edge of the abutments. The same figure shows the deformation of the bridge corresponding to the assumed mechanism. Our aim is to evaluate the reaction R_c of the central pier. Let us consider any settlement mechanism, v , and the corresponding kinematic reaction of the pier, denoted by μr defined by the equilibrium equation along v

$$\langle g, v \rangle + \mu \langle r, v \rangle = 0. \tag{a}$$

The corresponding kinematic multiplier, which depends on the position of hinge B, is thus given by

$$\mu(x) = - \frac{\langle g, v \rangle}{\langle r, v \rangle}. \tag{b}$$

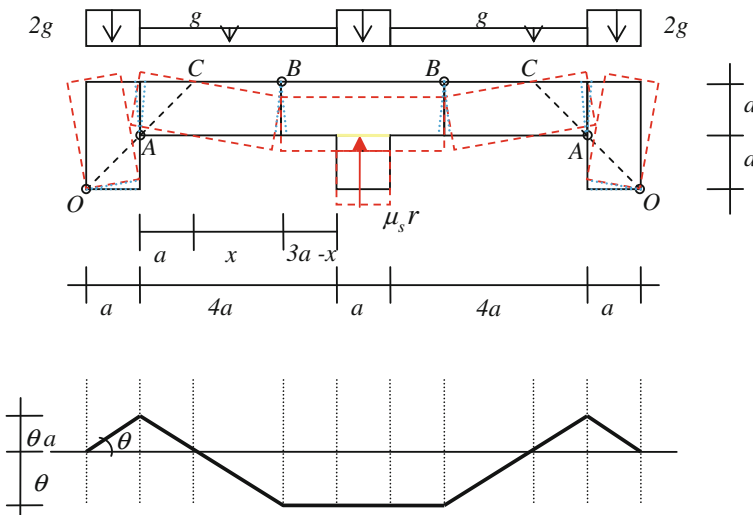


Fig. 2.51 A masonry bridge whose central pier has settled vertically

The actual pier reaction R_c can thus be obtained as the *maximum* of all kinematic reactions (b) by varying ν in the set of settlement mechanisms. We now evaluate the work, $\langle g, \nu \rangle$ and $\langle r, \nu \rangle$. The work of weight g along the mechanism is given by

$$\begin{aligned} \langle g, \nu \rangle &= 2\left[-2g \frac{a^2\theta}{2} - g \frac{a^2\theta}{2} + g \frac{x^2\theta}{2} + g(3a-x)x\theta + 2g \frac{ax\theta}{2}\right] \\ &= g(-3a^2 - x^2 + 8ax)\theta \end{aligned} \quad (c)$$

while the work $\langle r, \nu \rangle$ of the pier's reaction is $-x\theta$. According to (b), the kinematic reaction is thus given by

$$\mu r(x) = \frac{g(-3a^2 - x^2 + 8ax)}{x} \quad 0 \leq x \leq 3a, \quad (d)$$

depending on the position x of hinge B, which lies in the range $0 \leq x \leq 3a$. When $x \rightarrow 0$, $\mu r \rightarrow -\infty$, and for $x = 3a$, $\mu r = 4ga$ (Fig. 2.52).

The function $\mu(x)$ effectively reaches a *maximum* for $0 \leq x \leq 3a$. The value \bar{x} at which $\mu r(x)$ attains its maximum is thus obtained by solving the equation

$$\frac{d(\mu r)}{dx} = g\left(\frac{3a^2}{x^2} - 1\right) = 0, \quad (e)$$

which yields

$$x = \bar{x} = a\sqrt{3} \approx 1.73a. \quad (f)$$

The reaction of the central pier is evaluated by substituting (f) into (d), which yields

$$R_c = \mu r_{\max} = \mu r(x = a\sqrt{3}) = 2ga(4 - \sqrt{3}) \approx 4.54ga. \quad (g)$$

We will now show that the internal stress corresponding to the evaluated reaction is statically admissible. Figure 2.53 illustrates the equilibrium of the central part of the bridge, including the girder segments from hinges B to the pier.

Fig. 2.52 Finding the maximum of function $\mu r(x)$

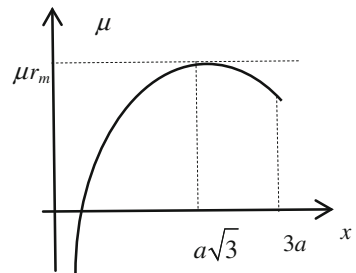


Fig. 2.53 Stress state around the central pier

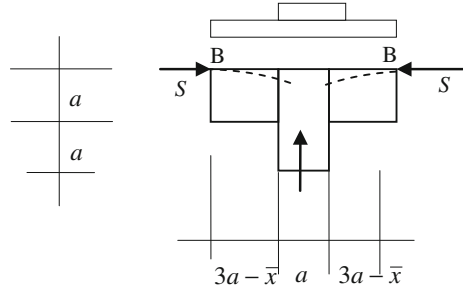
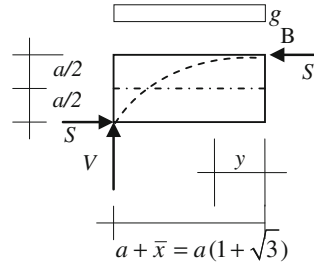


Fig. 2.54 Stresses in the span



The pressure line passes through hinge B and has a horizontal tangent at B. With the aim of evaluating the thrust, S , shown in the figure, let us examine the equilibrium of the portion of the girder between B and the abutment, as shown in Fig. 2.53. The length of this portion is $a + \bar{x} = a(1 + \sqrt{3})$ (Fig. 2.54). The shear force V transmitted to the abutment can be obtained via the equilibrium equation along the vertical direction:

$$V = ga(\sqrt{3} + 1).$$

We can also evaluate the thrust S . At $y = a + \bar{x} = a(1 + \sqrt{3})$, we have $Sa - g(a + \bar{x})^2/2 = 0$ and

$$S = \frac{ga}{2}(\sqrt{3} + 1)^2 = ga(2 + \sqrt{3}).$$

To obtain the corresponding pressure line, we can evaluate the moment acting at the section center located at distance y from B, which gives us

$$M(y) = S\frac{a}{2} - g\frac{y^2}{2} = g\frac{a^2}{2}(2 + \sqrt{3}) - g\frac{y^2}{2}.$$

The axial force N equals the thrust S , while the eccentricity of N is $M(y)/S$. Moreover, from the equilibrium along the vertical direction of the abutment, we get (Fig. 2.55)

Fig. 2.55 Stresses in the abutments

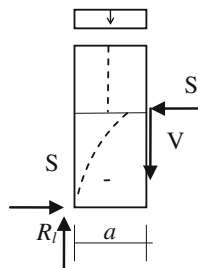
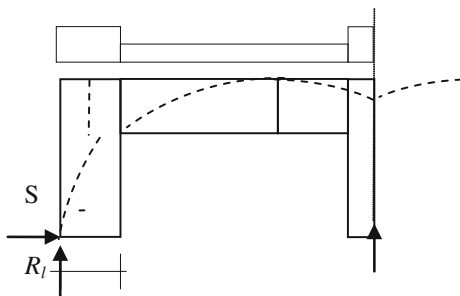


Fig. 2.56 The pressure line in the bridge



$$R_l = 2ga + V = 2ga + ga(\sqrt{3} + 1) = ga\sqrt{3}(1 + \sqrt{3}).$$

The abutment is loaded by a central axial force, N , from the head to midway along its height. Beneath this section the axial load varies and becomes $ga\sqrt{3}(2 + \sqrt{3})$, and its eccentricity ranges from 0 to $a/2$.

It can thus be concluded that the structure of the bridge, whose central pier has settled by $\sqrt{3}a\theta$ and is subject to the assumed loads and reaction $\mu r(\bar{x})$ at the base of the central pier, is in admissible equilibrium.

passing through the hinges of the settlement mechanism. The stress state is also statically admissible, thus proving that the thrusts, determined as the maximum of all kinematically admissible ones, is the sought for minimum thrust.

Figure 2.56 shows the overall pressure line on the entire structure of the bridge.

The minimum thrust can also be obtained by searching among the admissible funicular curves of the loads: the curve exhibiting the minimum slope at the sections where the girders join the central pier corresponds to this minimum.

2.7.8 Masonry Structures at Their Actual State

Limit Analysis, whose bases have been discussed above, offers the possibility of performing useful checks of the bearing capacity of masonry structures within the framework of the rigid no-tension model. However, Limit Analysis alone does not

provide the means to analyze the *actual* equilibrium state of a masonry structure. The admissible equilibrium equations alone are not enough to evaluate the internal stresses, as such problem is statically indeterminate.

To this end, other additional equations are required: the compatibility equations, as in the case of elastic structures. However, according to the rigid no-tension model, masonry structures cannot be deformed unless a mechanism is activated. Consequently, these supplementary equations cannot be formulated. Heyman (1995) however found that useful information can instead be obtained in the same context of the simple rigid no-tension model, that is, providing that the deformability of the constraints connecting the structure to the surrounding environment are taken into account. In brief, the assumption that settling of some constraints will inevitably occur may provide the required supplementary equations. Such an assumption generally reflects the *real behavior* of masonry structures, which frequently push against their supports that are in turn deformed by these thrusting actions. An arch or a dome, for instance, is inserted into a more complex structural system that must sustain their thrusts. These auxiliary structures undergo lateral deformations and can displace the springings of the arch or dome to follow their deformation. A minimal thrust state takes place in the arch or dome. The same occurs, for example, in the settling of the foundation of a masonry bridge pier. In many cases even a very thin crack can signal the occurrence of deformation.

The degree of settling can be predicted only with difficulty. Thankfully, the compatibility equations expressing the occurrence of settling do not require defining the magnitude of the settlement, but only indication of the constraints to the settled state. In more complex structures, as for instance a multi-span bridge or a masonry wall with openings, inspection of cracking patterns can provide useful information regarding the settlement mechanism effectively produced. According to this approach, determination of the actual stress state in masonry structures becomes statically determinate and Limit Analysis can once again be fruitfully applied, as will be shown. A number of useful applications of this approach will be described in later chapters.

2.8 Geometry and Strength: The Theory of Proportions of the Past Architecture

Masonry constructions have a long history. They have been built, studied, tested for about 7000 years but throughout all this time the material masonry, in spite of the large variety of its typologies, has maintained the same mechanical features. It is an unilateral material which can resist compression, but not tension.

This aspect has influenced the history of constructions and has marked out a forced path in the long research of the various structural solutions.

Construction experiences condensed during the time in the form of structural rules. The essence of these rules is that *proportion* controls the overall form of the

structure of the building. A Theory of Proportions developed slowly since Vitruvius up to Leon Battista Alberti and Palladio.

According to this theory Statics of masonry structures has to be ruled solely by geometry. Knowledge of the most suitable proportions amongst the various components of a structure and of their basic measure, *the modulus*, irrespective of its absolute magnitude, represented the essence of the art of past constructions. Since antiquity master builders have always used simple geometrical rules for designing arches or buttresses for a cross vault.

An ‘ideal city’ was conceived according these rules, as shown by the famous painting of an unknown artist of the fifteenth century (Fig. 2.57). Then, later, in the nineteenth century, masonry architecture felt into decay due the appearance of new materials and new structural forms.

Galileo confuted the rules of proportional design in his *Dialogues* (Fig. 2.58). Galileo observed that, given any structure which supports its own weight, if we multiply its size by a certain factor k maintaining its geometrical form, it becomes weaker.

To illustrate this statement by way of example, let us examine two similar beams a and A built with the same material and loaded by their own weights. The beam



Fig. 2.57 The ideal city conceived according to the “proportionality theory”

Fig. 2.58 The Galileo example of beam



A is k times larger than the beam a . In the transverse direction the beams have the same width s . Stresses σ and σ' in the beams a and A are respectively

$$\sigma = \frac{M}{W} \quad \sigma' = \frac{M'}{W'} = k\sigma \quad (2.162)$$

As a consequence, the beam A , as it grows in size, becomes weaker than the beam a . If we want maintain the same strength, the cross sections of the beam A must become thicker, as shown in the classical sketch of Fig. 2.59, taken from Galileo *Dialogues*.

Galileo realized that his discovery contradicted the rules of the proportional design of his days.

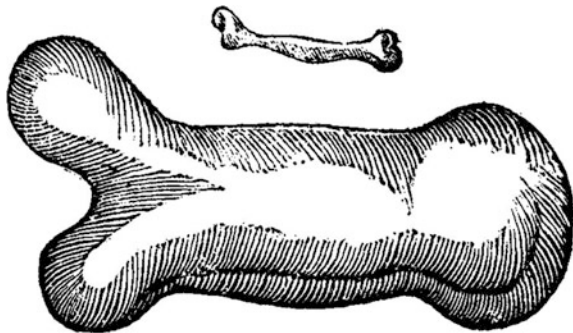
Some scholars, as Parson (1970), Benvenuto (1981), Mark (1990), identified in the Galileo judgement the irrefutable proof of the error rooted in the theory of proportions. On the contrary, for other scholars, as Dorn (1970), Heyman (1995), Baratta (1982) and Huerta (2001), the Galileo conclusion was not applicable to masonry constructions because for them the material strength plays no role.

We will show now, by means a direct proof and in the strict context of the no tension masonry model, that the Theory of Proportions is correct.

In previous sections we have seen that weight and geometry represent the essential elements in the strength of masonry structures. More precisely, it is *the proportions* among a structure's various constituent parts that define a its geometry, irrespective of the actual absolute dimensions.

To illustrate this by way of example, let us examine the two similar arches a and A in Fig. 2.60. Arch A , on the right, is k times larger than the arch a , on the left, or in other words, arch A is a k times *magnified copy* of arch a . In the transverse direction, i.e. in the direction orthogonal to their plane, the structures have the same width s . Each segment in structure A is thus k times longer than the corresponding segment in structure a . We can moreover consider other similar structures, such as s and S shown in Fig. 2.47, and refer to the same system of coordinate axes with origin O defined at the same position (Fig. 2.61). By definition, two points \mathbf{p}_i and \mathbf{P}_i , having respective coordinates (x_i, y_i) and (X_i, Y_i) , are *conjugated* if

Fig. 2.59 Larger thickness of the great bone in order to have the same strength of the small



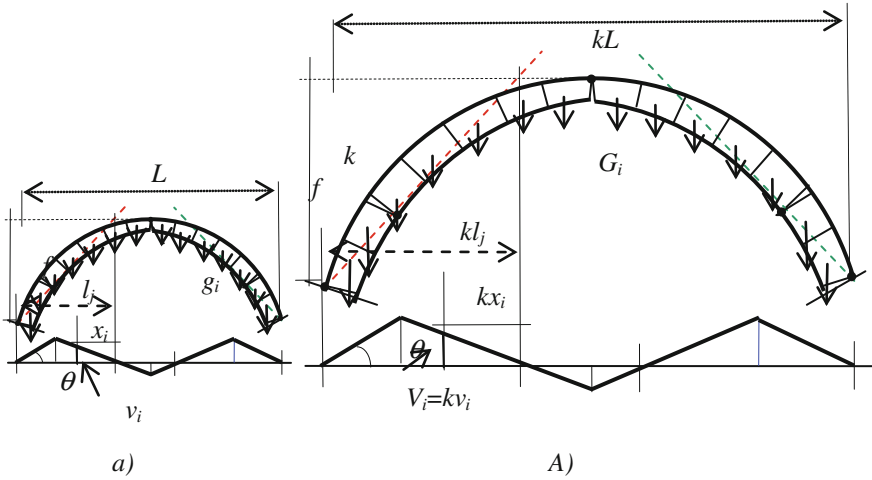


Fig. 2.60 Geometries of two similar arches and two corresponding mechanisms governed by dimension ratio k

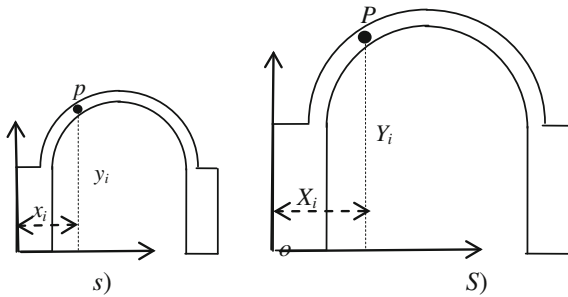


Fig. 2.61 Another example of two similar structures, s and S , in which the latter is the k times magnification of the former

$$X_i = kx_i \quad Y_i = ky_i. \tag{2.163}$$

So, the two arches a and A , for instance, are subdivided into an equal number of *conjugated* voussoirs v_i and V_i ($1, 2, \dots, i, \dots, N$), i.e. having centers having coordinates

$$(b_{xi}, b_{yi}) \quad (B_{xi}, B_{yi}) \tag{2.164}$$

with

$$B_{xi} = kb_{xi} \quad B_{yi} = kb_{yi}. \tag{2.163'}$$

At the same time the dimensions of the voussoirs c_i of arch a are length d_i and height h_i , while those of voussoirs C_i of arch A are D_i and H_i ($i = 1, 2, \dots, N$), with

$D_i = k d_i$ and $H_i = k h_i$. Consequently, if g_i and G_i are the weights of the voussoirs, we have

$$G_i = k^2 g_i. \tag{2.165}$$

Let us now consider the *conjugated mechanisms* m and M , respectively for structures s and S : the latter is the k magnification of the former. The two mechanisms present the same rotation parameter θ and their hinge points \mathbf{c}_i and \mathbf{C}_i are conjugated. Hence, if l_j is the distance of the hinges of the arch a mechanism from the left springing, the corresponding distance of the hinges of arch A will be kl_j , and the lines connecting the two corresponding hinges are parallel to each other, as shown in Fig. 2.60. The centre, \mathbf{b}_i , of voussoir i of the arch a , being at distance x_i from the corresponding point of rotation, moves vertically by v_i .

Likewise,

$$V_i = k v_i. \tag{2.166}$$

and kx_i are the vertical displacement and analogous distance of centre \mathbf{B}_i of the corresponding voussoir i of arch A . Let us now assume that structure a is *stable* under its own weight g , as defined according to (2.71'),

$$\langle g, v \rangle = \sum_1^N g_i v_i < 0 \tag{2.167}$$

for any mechanism v . The work $\langle g, v \rangle$ is evaluated considering the work of the weight forces g_i on the corresponding vertical displacements v_i of the mechanism.

We will now show that the k magnified structure A is thus also *stable* under its own weight, in the sense that, analogously for any mechanism V , we will have

$$\langle G, V \rangle = \sum_1^N G_i V_i < 0. \tag{2.167'}$$

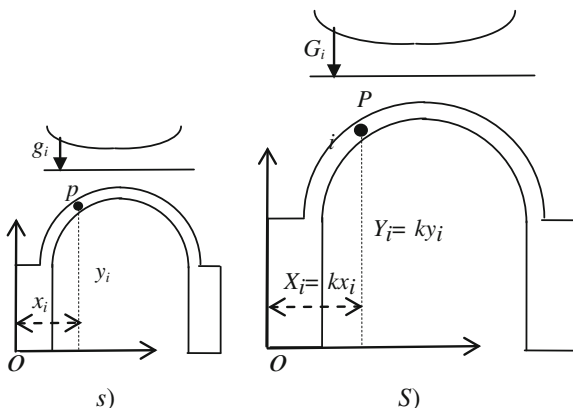
In fact, according to the foregoing assumptions and definitions, due to the similarity between s and S and associated mechanisms m and M from (2.127) and (2.128)

$$\langle G, V \rangle = \sum_1^N G_i V_i = k^3 \sum_1^N g_i v_i < 0. \tag{2.168}$$

Thus, to conclude, *if a structure under its own weight is stable, a k times magnified copy will also be stable.*

The *same* outcome holds in a more general sense. Let us consider the two similar structure s and S of Fig. 2.62 where now *only* the weights, g_a and G_a , of their central spans increase via loading parameters λ and Λ . According to the kinematic approach, the maximum load $\lambda_o g_a$ that structure s can sustain (see Sect. 2.6.3) can be obtained as

Fig. 2.62 The k similar structures loaded by increasing weights along their spans



$$\lambda_o = \text{Min} \left(- \frac{\langle g, v \rangle}{\langle g_a, v \rangle} \right) = \text{Min} \left(- \frac{\sum g_i v_i}{\sum g_{ai} v_i} \right) \quad v \in M \quad (2.169)$$

where g is the pier weight and g_{ai} and g_i the corresponding weights of the voussoirs into which the structure has been divided. Likewise, the maximum load $\Lambda_o G$ that the k magnified structure S can sustain is

$$\Lambda_o = \text{Min} \left(- \frac{\langle G, V \rangle}{\langle G_a, V \rangle} \right) = \text{Min} \left(- \frac{\sum G_i V_i}{\sum g_{ai} V_i} \right) \quad V \in M. \quad (2.170)$$

However, according to previous assumptions

$$G_i = k^2 g_i. \quad G_{ai} = k^2 g_{ai} \quad V_i = k v_i, \quad (2.171)$$

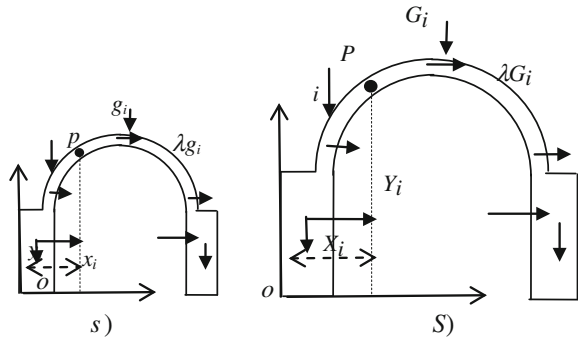
and the two structures s and S exhibit the same strength under loads λg and ΛG . In fact, we have

$$\Lambda_o = \text{Min} \left(- \frac{k^3 \sum g_i v_i}{k^3 \sum g_{ai} v_i} \right) = \lambda_o. \quad (2.172)$$

This result holds even if we consider that, instead of *vertical* loads λg , there are *horizontal* forces λg , still proportional to weight g , acting on the structure. Such a loading condition is frequently considered representative of *seismic* actions. The two similar structures s and S in Fig. 2.63 thus exhibit the same horizontal strength under the action of horizontal forces λg and ΛG .

These results, here directly proved, were well known to architects of the past and formed the basis for their fundamental rules of construction. As set down in the theory of proportions by Andrea Palladio and Leo Battista Alberti, the statics of masonry structures is governed solely by their geometry and, consequently, by their basic measurement, the modulus, irrespective of their absolute measurements

Fig. 2.63 Similar structures under horizontal load λg and λG



Knowledge of the most suitable proportions amongst the various components of a masonry structure (knowledge often jealously guarded by past masters) represented the essence of the art of construction.

As discussed throughout this book, these results, arrived at through centuries' long experience, is a direct consequence of the unique, fundamental behavior of masonry. By way of example, Iori (2009) has recalled two Romans dome constructions: the Pantheon and the Temple of Romulus, similar but different in scale (Fig. 2.64). Both the constructions have the maximum height equal to the dome diameter and a drum thickness equal to 0.3 of the radius.

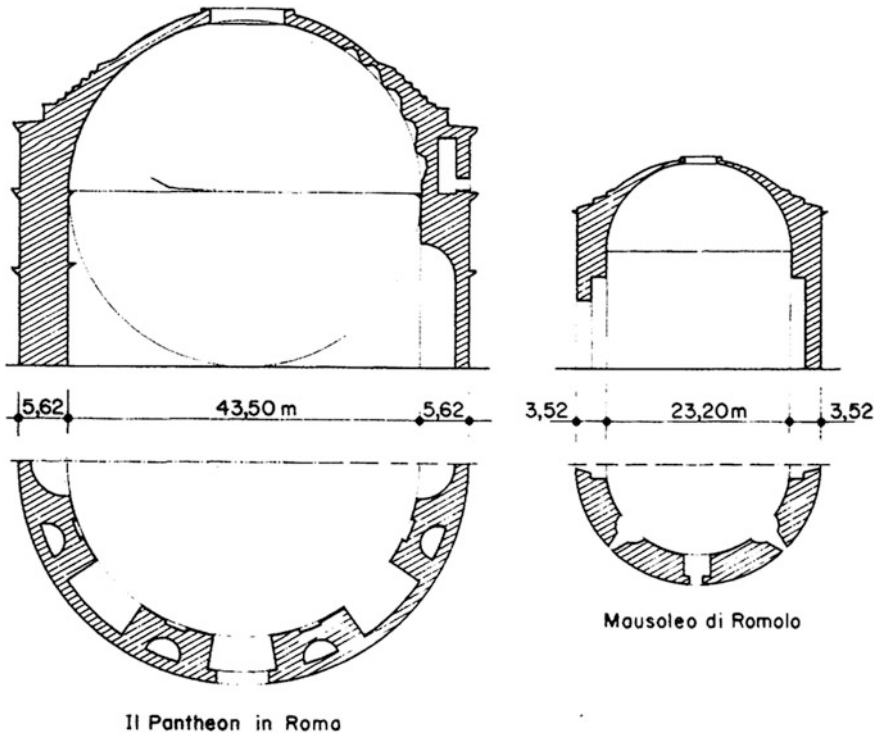


Fig. 2.64 The Pantheon in Rome and the Temple of Romulus (Iori 2009)

Appendix

A.1 Lessons from the Failure of Cathedral of Noto

The Church

In order to better illustrate the foregoing basic assumptions regarding the behavior of masonry structures, it is useful to analyze the causes of the 1996 collapse of the Cathedral of Noto (Sicily). The Noto cathedral has two side aisles and a central nave. The beautiful 40 m-wide, 32 m-high baroque facade is flanked by two bell towers, as shown in Fig. 2.65.

The bases of the towers and facade are 3.40 m below the level of the Church floor (assumed to be at 0.00 m). The tower's foundations are partially exposed near the side streets due to some excavation work done in the late 19th century. The lateral walls of the Church are faced with regular blocks and mortar beds, while rubble masonry with poor mortar makes up the walls' inner cores. The five piers that run alongside the central nave, are similar in structure to the lateral walls: facings made of regular square blocks of local travertine with inner rubble masonry (Fig. 2.66). Only their bases were built with the more substantial Noto limestone.

The piers have a roughly rectangular cross section, 3.25 m \times 1.60 m, with their main lengths laid along the church's longitudinal direction. The piers sustaining the dome at the transept are larger in cross section: 6.50 m \times 1.65 m.

The side aisles are roofed by small domes set on small drums, in turn, sustained by the side walls and longitudinal and transverse arches spanning from walls to piers (Figs. 2.66 and 2.67). All the domes and arches of the aisles have a thick inner rubble structure and regular facings with squared stone blocks.

A long wall running along the top of the interior piers sustains a reinforced concrete floor that was built to replace the original wooden roof during past restructuring work. Fortunately, the operations spared the high transverse masonry arches spanning the nave. The spherical dome, with an inner diameter of 11.20 m

Fig. 2.65 Cathedral façade



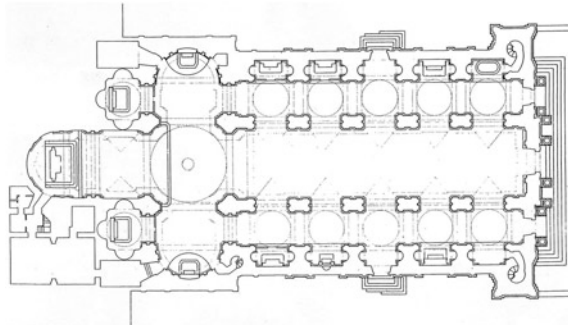


Fig. 2.66 The plan of the Cathedral

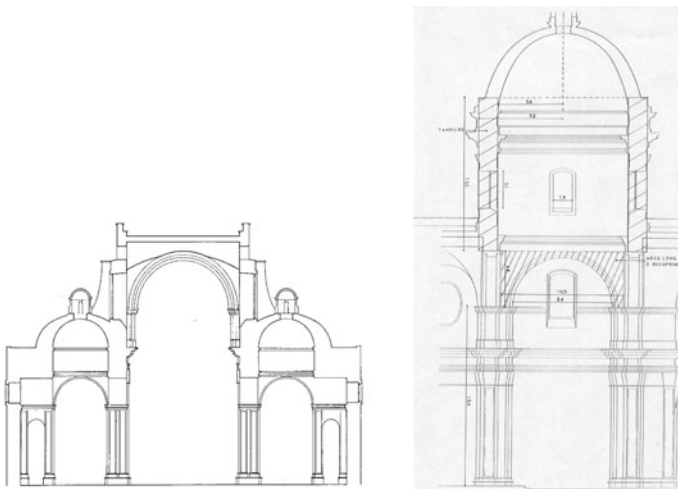


Fig. 2.67 Cross section of the church at the nave and transept

was built using strong blocks of Modica limestone on top of a drum containing several large windows. The dome and drum were 1.30 m thick. The foundations of the church's lateral walls are made up of continuous masonry walls set on a thick formation of sandstone and clays. The more superficial foundations of the piers rest on an arenaceous formation 1 m beneath the level of the church floor.

Construction of the Cathedral was begun in 1753 and completed in 1769. The dome has collapsed a number of times: first during its construction, a second time during an 1848 earthquake, after which it was rebuilt for the third time between 1860 and 1862 and remained up to the most recent collapse in 1996. It has since been reconstructed. In 1990 an earthquake measuring 4.7 on the Richter scale struck the entire region of Syracuse and seriously damaged many structures of the church. In the area of Noto the damage was rated at level VI on the Modified Mercalli Intensity scale (MMI). The Church was seriously damaged in the earthquake: the

transverse arches together with the aisle roofs suffered deep cracking, particularly on the right aisle. Afterwards, some damaged piers were buttressed with simple scaffolding and the church remained open while its condition continued to worsen, until its near complete collapse in 1996.

The 1996 Collapse

The failure occurred suddenly, without any storm or earthquake, and affected the entire interior of the church. All the piers and coverings of the right nave collapsed together with the dome. Only the beautiful façade was spared. Figure 2.68a, b show the interior of the cathedral with the remnants of the dome after the collapse.

Investigations of the Causes of the Failure

A committee appointed by the Court of Syracuse, composed of M. Como, G. Croci, M.T. Lo Balbo, A. Migliacci, and F. Selleri, carried out a survey to ascertain the cause of the collapse (1998, 2001). Compression strengths of the various stones: local travertine: $\sigma_{rm} = 61 \text{ kg/cm}^2$; Noto limestone, $\sigma_{rm} = 195 \text{ kg/cm}^2$; giuggiulena stone, $\sigma_{rm} = 95 \text{ kg/cm}^2$; Modica limestone, $\sigma_{rm} = 220 \text{ kg/cm}^2$.



Fig. 2.68 a The interior of the church after collapse; b The collapsed dome

Fig. 2.69 Upper fragment of pier 4



Fig. 2.70 The base of pier 4, weakened by the passageway to the pulpit



After all the various investigations, geotechnical drillings, material testing and ground-penetrating radar explorations, it became possible to examine the bases of the failed piers as soon as the rubble was completely cleared (Figs. 2.69 and 2.70).

The Structural Collapse: How Can We Explain the Failure?

Despite the presence of many cavities in the soil beneath the church floor, accurate numerical and geotechnical investigations excluded the possibility that settling of the foundation had occurred, a conclusion that was also confirmed by visual

inspection of the pier bases. The elements that were fundamental to enabling definition of the failure kinematics were the counter rotation of the upper parts of the failed piers near the transept and the sequence of cracks that signalled failure of the upper reinforced concrete ring beam. Figure 2.71 shows the strong wrenching action exerted on the reinforced concrete ring beam running along the top of the upper wall lining the nave, revealing the point where the collapse started—precisely at the position of pier n. 4. This pier was weaker than the others due to the presence of an old interior passageway providing access to the pulpit (Fig. 2.70). The presence of the overhead transverse arches at the level of the roof over the nave determined a two-hinge mechanism, one at the pier base and the other high up at the springing of the transverse arch. This mechanism caused counter-rotation of the upper part of the piers, which was in effect confirmed by examination of the position of the parts of the failed piers (Fig. 2.69). The structure of the cathedral was thick and resistant. In particular, the transverse arches, drums and small domes roofing the aisles, constructed with heavy concrete (Fig. 2.74), give the impression of a solid monolithic structure. The roofs also gave the appearance of behaving as a single unified mass, able to transmit only axial loads to their supports.

However, contrary to appearances, these thick roofing structures were actually particularly vulnerable. The concrete had very little tensile strength, so these structures were able to sustain their own weight and transmit it to the underlying piers only as long as the concrete was intact. However, if its strength were to decay, for instance due to damage from sudden seismic actions or slow masonry decay by the action of rainwater seeping into the masonry, the behavior of the structure would change drastically (Fig. 2.72).

Fig. 2.71 Cracking of the ring beam showing the strong pulling action due to the collapse of underlying pier 4



Fig. 2.72 The massively thick concrete of the arches and small domes



In fact, the 1990 earthquake caused extensive damage to many of the cathedral's structures. Alarming cracks appeared in its support structures, especially on the right side. When the thick structures covering the right aisle cracked, their monolithic behavior was lost and strong thrusts were activated. Static checks of the piers lining the nave revealed that the compression stresses acting upon them were admissible only for the heavy vertical loads acting alone; if instead the action of the

Fig. 2.73 The failure mechanism

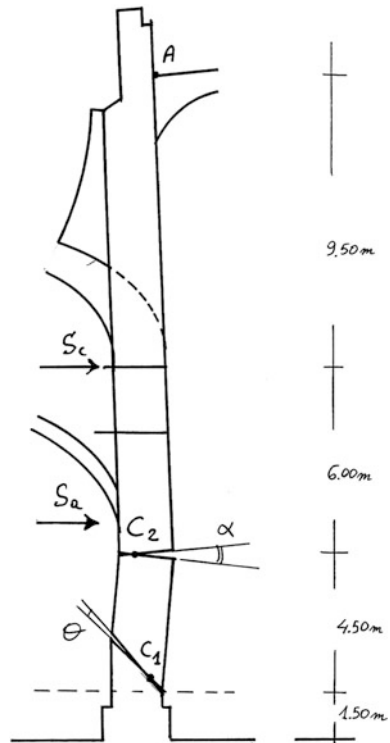
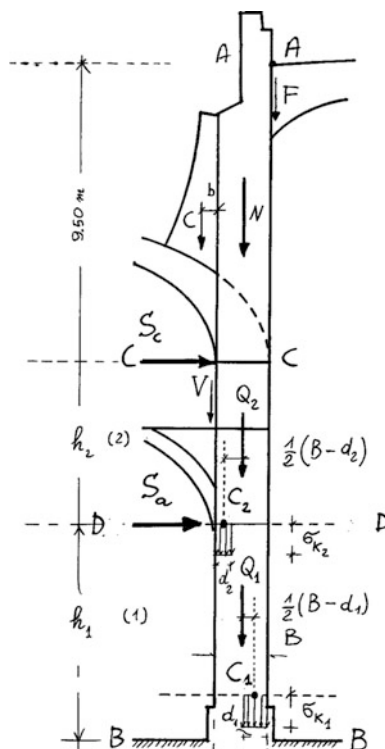


Fig. 2.74 The limit equilibrium of the pier



thrusts of the domes and arches were taken into account, the check showed that the piers were at the very limit for failure. Figures 2.73 and 2.74 show the collapse mechanism and the distribution of thrusts and internal stresses of pier n.4.

Lesson to Be Learned from the Failure

The lesson imparted by the failure of the Noto Cathedral serves as confirmation that, in the interplay between weight and geometry, only the no-tension model can provide reliable indications as to the true strength of masonry structures. Thus, although a certain amount of tensile strength may be allowed for, in the end, it is the no-tension model that best predicts the true behavior of masonry structures.

We must therefore distinguish between structures that are *intrinsically stable*—that is, those that, given their geometry and load distribution, can sustain the loads within the assumptions of no-tension behavior—and those that are instead *intrinsically unstable*—unable to sustain such thrusts under the no-tension model.

In this sense, the structure of the cathedral was intrinsically unstable. Unfortunately, the apparent solidity of the vaulted concrete systems was

misleading. In fact, once the thrusts of the arches and domes covering the right aisle were activated by the cracking, the piers were unable to sustain these thrusts and consequently collapsed.

Ironically, the church's collapse could have been avoided by simply fixing chains under the transverse arches and right aisle domes just after the damage caused by the 1990 earthquake.

The cathedral of Noto has since been rebuilt and currently represents one of the most extraordinary examples of baroque architecture in Italy, particularly in its magnificent façade.

References

- Angelillo, M., Cardamone, L., & Fortunato, A. (2010). A new numerical model for masonry like structures. *Journal of Engineering and Material and Structures*, 5.
- Baratta, A., & Toscano, R. (1982). Stati tensionali in pannelli di materiale non resistente a trazione, AIMETA, National Conference, Genova.
- Benvenuto, E. (1981). *La Scienza delle Costruzioni e il suo sviluppo storico*. Roma: Firenze, Sansoni, Ristampa, Edizioni di Storia e Letteratura.
- Benvenuto, E. (1991). *An Introduction to the history of structural mechanics, part ii, vaulted structures and elastic systems*. NY: Springer-Verlag.
- Briccoli, B.S., Paradiso, M., & Tempesta, G. (1988). Analisi Statica, Cinematica ed Equilibrio Limite di Strutture ad arco a Vincoli unilateri, IX Congr. Naz.le AIMETA, University of Bari, 4–7 Ott., Tipolito Il Globo, Bari.
- Como, M., & Grimaldi, A. (1985). An unilateral model for the limit analysis of masonry walls. In *International Congress on Unilateral Problems in Structural Analysis, Ravello, 1983, CISM Udine*. Springer Verlag.
- Como, M. (1992) Equilibrium and collapse of masonry bodies. *Meccanica*, 27, 185–194. Kluwer Academic Publications, London.
- Como, M. (1996a). *On the role played by Settlements in the Statics of Masonry Structures in the Conference Geotechnical Engineering for the Preservation of Monuments and Historic sites, Napoli, Italy*, 3–4, October. Rotterdam: A.A. Balkema.
- Como, M. (1996b). In Pitagora (Ed.), *Multiparameter Loading and Settlements in Statics of Masonry Structures, Proceedings Conference Meccanica delle Murature tra teoria e progetto*, Messina, 18–20 September 1996, Bologna.
- Como, M. (1998) Minimum and maximum thrust states in Statics of ancient masonry buildings. In *Proceedings 2nd International Arch Bridge Conference*, Venice, Italy, 6–9 October. Sinopoli, Rotterdam: A.A. Balkema.
- Como, M. (2012). On the statics of bodies made of compressionally rigid no tension materials. In M. Fremond & F. Maceri (Eds.), *Mechanics, models and methods in civil engineering*. Berlin Heidelberg: Springer Verlag.
- Como, M., Croci, G., Lo Balbo, M.T., Migliacci, A., & Selli, F. (1998). sintesi a cura di, tratta da *Consulenza Tecnica sulla Chiesa Madre San Nicolò di Noto*, Proc. della Repubblica presso il Tribunale di Siracusa.
- Como, M., Croci, G., Lo Balbo, M.T., Migliacci, A., & Selli, F. (2001). Problematiche ed indagini sul crollo nella Cattedrale di Noto del 13–03–1996, Atti del Convegno Nazionale *Crolli e Affidabilità delle Strutture Civili*, IUAV, Venezia.
- Coulomb, C.A. (1821). Essai sur une application des règles..., *Mémoires de Mathématique et de Physique*, présentés à l'Académie Royale des Sciences, Vol. 17, 1773, pp. 343–382. Paris 1776, reprinted in *Theorie des machines simples*, Paris.

- Del Piero, G. (1989). Constitutive equation and compatibility of the external loads for linear elastic masonry-like materials. *Meccanica*, 24, 150–162.
- Di Pasquale, S. (1984). *Statika dei solidi murari: teorie ed esperienze*, Atti del Dipartimento di Costruzioni, Università di Firenze.
- Di Pasquale, S. (1996). *L'Arte del Costruire, Tra conoscenza e scienza*, Ed. Marsilio, Venezia.
- Drucker, C. K. (1959). A definition of stable inelastic material. *Journal of Applications Mechanics*, 26, 1.
- Fontana, C. (1694). *Il tempio vaticano e la sua origine*, Roma.
- Bacigalupo, A. & Gambarotta, L. (2011). Non-local computational homogenization of periodic masonry. *International Journal Multiscale Computational Engineering*, 9.
- Giuffrè, A. (1990). *Lecture sulla Meccanica delle Murature Storiche*. Roma: Facoltà di Architettura dell'Università di Roma La Sapienza.
- Giuffrè, A. (1991). *La meccanica nell'Architettura, La statica*. Roma: La nuova Italia Scientifica.
- Heyman, J. (1966). The stone skeleton. *Intern. Journ. Solids Structures*, 2, 249.
- Heyman, J. (1982). *The masonry arch*. Chichester: Ellis Horwood.
- Heyman, J. (1995). *The stone skeleton, structural engineering of masonry architecture*. Cambridge: Cambridge University Press.
- Horne, M.R. (1971). *Plastic Theory of structures*, T. Nelson and Sons Ltd, London.
- Huerta, S. (2001). Mechanics of masonry vaults: The equilibrium approach. In P.B. Lourenco & P. Roca (Eds.), *Proceedings 3rd International Semester on Historic Constructions*, Guimaraes, Portugal, University of Minho.
- Kooharian, A. (1952). Limit analysis of vousoir (Segmental) and concrete arches. *ACI Journal* (December, Proc. V, 49).
- Iori, I. (2009). Il quadro storico-scientifico in *Santa Maria del Quartiere in Parma, Storia, rilievo e stabilità di una fabbrica farnesiana* a cura di Giandebiaggi P., Mambriani C., Ottoni F., University of Parma, Fondazione Cariparma, ed. Grafiche Step, Parma.
- Lucchesi, M., & Zani, N. (2003). Some explicit solutions to plane equilibrium problem for no-tension bodies. *Structural engineering and Mechanics*, 16(3), 295–316.
- Lucchesi M., Padovani C., Pasquinelli G., & Zani N (2008). *Masonry Constructions: Mechanical Models and Numerical Applications*, Lecture Notes in Applied and Computational Mechanics (Vol. 39). Berlin Heidelberg: Springer.
- Ochsendorf, J. (2006). The masonry arch on spreading supports. *The Structural Engineer*, 84(2).
- Prager, W. (1959). *An Introduction to Plasticity*. U.S.A: Addison Wesley Publications, Reading, Mass.
- Romano G., & Romano M. (1985). Elastostatics of sstructures with unilateral conditions on strains and displacements. In *Intern. Congr. On Unilateral Problems in Struct. Analysis'*, Ravello 1983, CISM, Springer.
- Romano G., & Sacco E. (1986) Sul calcolo di strutture murarie non resistenti a trazione, *Atti Istit. Scienza delle costruzioni*. Università di Napoli.
- Sinopoli, A., Corradi, M., Foce, F. (1998). Lower and upper bond theorems for masonry arches as rigid systems with unilateral contacts. In *Proceedings 2nd International Arch Bridge Conference, Venice, Italy, 6–9 October*. Rotterdam: A.A. Balkema.
- Trovalusci, P. (1993). Sulla modellazione meccanica dei solidi murari. In *Sicurezza e conservazione dei centri storici. Il caso di Ortigia*, a cura di A.Giuffrè, Laterza, Bari.
- Trovalusci, P., & Masiani, R. (2005) A multifield model for blocky materials base on multiscale description. *Int.mJ. Solids and Structures*, 42.
- Viollet-le-Duc, E.E. (1854–1868). *Dictionnaire raisonné de l'architecture*, Paris.
- Vol'pert, A. I., Hudjaev, S. I. (1985). *Analysis in Classes of Discontinuous Functions and equations of Mathematical Physics*, Nijoff.



<http://www.springer.com/978-3-319-24567-6>

Statics of Historic Masonry Constructions

Como, M.

2016, XVIII, 619 p. 592 illus., 112 illus. in color.,

Hardcover

ISBN: 978-3-319-24567-6